

Organic geochemical characterization of deltaic Paleogene rock units in Coos Bay, Oregon: Kerogen type and richness in response to depositional environments

Allison K. Barbato, John M. Armentrout, Leslie B. Magoon, Thomas Demchuk, Craig Barrie, and Sophie Warny

ABSTRACT

Coastal depositional environments are known to host source, reservoir, and seal rocks. The middle Eocene Coaledo Delta in Coos Bay, Oregon, with its well-preserved coastal units, has been identified for its potential to generate and accumulate petroleum. Previously encountered gas implies that a viable, gas-prone source rock exists in the Coos Bay area. This study assesses 84 outcrop and 12 core samples from Coos Bay using parameters such as total organic carbon (TOC), hydrogen index (HI), thermal maturity (T_{max}), and organic petrography to elucidate which formation likely produced the encountered gas. Results were integrated with lithologic observations to relate geochemical changes to depositional environments over time.

Results indicate that the Lower and Upper Coaledo contain organic-rich coal seams and siltstone that are the most prospective gas-prone source rock units, with kerogen sources ranging from terrigenous to marine. The samples are generally immature, potentially suggesting gas migration from depth. Laminated mudstones exhibit higher average TOC and HI values compared to bioturbated mudstones, but HI appears to be more affected. Substantial discrepancies between outcrop and core geochemistry are evident, with free hydrocarbon (S_1) core data ~55% higher and remaining generative potential (S_2) core data ~90% higher. Although part of this variance is attributed to weathering,

Copyright ©2024. The American Association of Petroleum Geologists. All rights reserved.

Manuscript received January 25, 2023; provisional acceptance June 5, 2023; revised manuscript received November 14, 2023; revised manuscript provisional acceptance January 22, 2024; 2nd revised manuscript received January 24, 2024; final acceptance January 25, 2024; preliminary ahead of print version published April 1, 2024.

DOI:10.1306/01252423011

AUTHORS

ALLISON K. BARBATO ~ *Department of Geology and Geophysics, Louisiana State University, Baton Rouge, Louisiana; Museum of Natural Science, Louisiana State University, Baton Rouge, Louisiana; allison.barbato@gmail.com*

Allison K. Barbato, a Ph.D. student at Louisiana State University (LSU), integrates biostratigraphy and source rock geochemistry to study Paleogene deltaic environments. As president of the LSU AAPG Chapter and a recipient of the Chevron Energy Leaders Scholarship, she increased membership in the chapter by 400% and successfully mentored students toward career opportunities. She graduates in 2024 and will work with Chevron in Houston, Texas. She is the corresponding author of this paper.

JOHN M. ARMENTROUT ~ *Department of Earth Sciences, University of Oregon, Eugene, Oregon; jarmenrock@gmail.com*

John M. Armentrout is a research associate with the University of Oregon, where he is coordinating an interdisciplinary study of the Coos Bay Basin. He received his M.S. degree at the University of Oregon in 1967 and his Ph.D. in 1973 from the University of Washington. From 1973 to 2000, John worked for Mobil Oil Corporation. Since retiring, he has consulted and taught part-time.

LESLIE B. MAGOON ~ *Department of Geological Sciences, Stanford University, Stanford, California; lesmagoon@gmail.com*

Leslie B. Magoon is an adjunct professor at Stanford University. He received his M.S. degree in geology in 1966. He worked at Shell Oil Company and for the US Geological Survey. Since 1981, he has popularized the petroleum system through talks, courses, and AAPG Memoir 60, *The Petroleum System—From Source to Trap* (1994). He received the Sidney Powers Memorial Award in 2021.

THOMAS DEMCHUK ~ *PetroStrat, The Woodlands, Texas; thomas.demchuk@petrostrat.com*

Thomas Demchuk is an adjunct professor in the Department of Geology and Geophysics at LSU. He is a business development manager and geological consultant with PetroStrat in Houston, Texas, marketing specialist geology products to the energy community. He received his Ph.D. in 1992 from the University of Calgary. He has ~30 years of experience in the oil industry.

CRAIG BARRIE ~ *GeoMark Research, Houston, Texas; present address: Applied Petroleum Technology, Oslo, Norway; craig.barrie@apt-int.com*

Craig Barrie is chief operating officer at Applied Petroleum Technology. He holds a Ph.D. in geochemistry from Liverpool University (2008) and a B.Sc. degree in geology from Glasgow University (2005). Since earning his Ph.D., he has held fellowships at the Universities of St Andrews and Glasgow before joining industry in 2011. He is a subject matter expert in isotope geochemistry and has published more than 40 technical papers.

SOPHIE WARNY ~ *Department of Geology and Geophysics, Louisiana State University, Baton Rouge, Louisiana; Museum of Natural Science, Louisiana State University, Baton Rouge, Louisiana; swarny1@lsu.edu*

Sophie Warny is a professor of palynology at LSU in Baton Rouge. She received her Ph.D. in 1999 from the Université Catholique de Louvain in Belgium. Since being hired at LSU in 2008, she has directed 30 graduate students on various Cretaceous to Cenozoic sections. Most of her former students are now employed in the oil and gas industry.

ACKNOWLEDGMENTS

This paper is part of a doctoral research project. The lead author is funded by a LSU graduate student fellowship and a series of awards, including the Houston Geological Society W. L. Calvert Memorial Scholarship, an AAPG Grants-in-Aid award, the LSU AAPG Student Chapter, the George and Clare Hart Fellowship, the Chevron Energy Leaders Scholarship, the Mary Jo Klosterman Superior Graduate Student Scholarship, the American Association of Stratigraphic Palynologists Center for Excellence in

lithology and depositional environments may also play a role. Furthermore, this study discusses the importance of a hierarchical approach to filtering S_2 data for the determination of T_{max} . This involves evaluating S_2 peak morphology using statistical descriptors such as bimodality, skewness, and kurtosis in combination with an $S_2 > 0.15$ mg HC/g rock.

INTRODUCTION

Geologic environments known to create conditions needed to accumulate and trap hydrocarbons (HCs) include shelf-margin depositional systems, which are globally recognized as having essential elements of the petroleum system, such as source, reservoir, and seal rocks (Magoon and Dow, 1994). The middle to late Eocene Coaledo Delta and its associated prearc to forearc shelf-margin depositional units (Diller, 1901; Dott, 1966) have been identified in the Coos Bay area on the southwestern coast of Oregon as having the potential to be an effective petroleum system (Figures 1–5).

The nearly 5000 m (16,000 ft) composite Paleogene section contains exceptionally preserved Eocene–Oligocene deltaic and shallow-to-deep marine sediments, encapsulating shoreface to distal prodelta gravity-flow sandstone encased in marine mudstones (Figures 4, 5). Many of these lithic feldspathic sandstones have fair porosity and permeability (Van Atta, 1980; Chan, 1985). In addition, the commercial petroleum potential of Eocene sandstone reservoir rocks has been proven in the coastal regions of Oregon in the Mist gas field, where late Eocene basaltic intrusions are inferred to have matured coaly source rock facies to generate the trapped gas (Newton, 1979, 1980; Olmstead, 1985; Stormberg, 1991).

However, continued exploration in the coastal Oregon region after the initial Mist gas field discovery has resulted in only a few HC shows and no commercial discoveries to date (Brownfield, 2011; Curzon Energy, 2022). Geochemical analyses by Tybor (1980) analyzed eight surface samples with total organic carbon (TOC) values <0.75 wt. %, except for one coal at 50.14 wt. % TOC. Haykus (1980) studied 10 surface samples with TOC values from marine facies reporting values below 0.86 wt. %. However, the lack of exploration success has been attributed to the incomplete understanding of the regional HC potential, especially as it relates to source rock richness and regional thermal maturation trends (Armentrout and Suek, 1985; Snavely, 1987; Stanley, 1991; Stormberg, 1991; Ryu, 2008). Exploration wells drilled in the 1960s tested offshore HC potential, finding only gas shows. The public well reports do not include geochemical data. Postdrilling assessment suggested the absence of thermally mature organic-rich potential source rock, thus encouraging deeper

drilling. Also considered were possible well locations that were too high on structures, thus missing flank reservoir sandstone (Newton, 1979). Assessment of potential resources in the Pacific Northwest is provided by Brownfield (2011) and economic evaluation is provided by Profita and Schick (2022).

Since 1980, no new data that relate to the geochemical characterization of Coos Bay area rock units have been published (Newton, 1980). However, advances in source rock characterization methodologies have evolved, becoming increasingly more accurate and reliable (Curiale and Curtis, 2016). The present study reevaluates the source rock potential of the rock units and their depositional environment in the Coos Bay area using modern source rock evaluation techniques. This study analyzes 96 new samples for organic richness (*TOC wt. %*), kerogen type, or quality (hydrogen index [*HI*] mg HC/g *TOC* and organic petrography), and thermal maturity (T_{max}).

REGIONAL GEOLOGY AND PALEOGEOGRAPHY OF COOS BAY

Regional Geology and Tectonics

New investigations of the Coos Bay forearc basin in southwestern Oregon have established a revised chronology and kinematic history of basin development and its relationship to the rest of the Cascadia forearc following the accretion of the Siletzia forearc basement (Figure 3; Armentrout et al., 2021; Dorsey et al., 2021; Wells and Niem, 2021; Darin et al., 2022). Detrital zircon ages provide refined stratal correlations suggesting that the Oregon postcollisional Paleogene basin was a single depositional area punctuated by local and subregional unconformities (Figures 2, 3, 5).

Siletzia, an oceanic basaltic plateau extruded circa 55–50 Ma on the Farallon Plate, docked with North America in the early Eocene (ca. 51–49 Ma; Wells et al., 2014). Deformation due to Siletzia's docking created the Paleogene syncollisional foredeep Umpqua Basin (Dorsey et al., 2021). Following this, the onset of Cascadia subduction is estimated at circa 49–46 Ma, which was then followed by volcanic arc eruptions in the southern Cascades at circa 42–40 Ma (Retallack et al., 2004; Bindeman et al., 2021; Dorsey et al., 2021). During the transition period between tectonic accretion and arc flare-up, the Coaledo Delta began to develop on the southwestern coast of Oregon into a northwest-facing forearc basin. Throughout the Paleogene, the Cascadia forearc basin (≤ 48 to ≥ 31 Ma) exhibited northward prograding deposition at present-day coordinates (Snively et al., 1964; Dott, 1966; Santra et al., 2013). This progradation, guided by margin-parallel extension during the Tillamook magmatic episode (Figure 3), led to successive

Palynology CENEX Chair Fund, and the Kae and John Armentrout Fellowship at the LSU Foundation. In addition, the authors thank GeoMark Research Ltd. and the Stanford University Geology Department, Basin and Petroleum System Modeling Affiliates Program for their gracious financial support. The authors are grateful to Barry Katz, AAPG Editor Matthew J. Pranter, and two anonymous reviewers for their constructive feedback that helped improve the manuscript. Lastly, we thank Joe Curiale of Geochemical Advisory Services for his valuable discussions and geochemical insight, Cortland Eble of the Kentucky Geological Survey for his time spent preparing the sample pellets used for this study, and Mike Darin of the Oregon Department of Geology and Mineral Industries for his input. For more on the Coaledo Project research effort, visit <https://www.gsoc.org/news/2019/7/10/he-coaledo-project-revisits-the-formation-of-the-south-central-oregon-coast> for "The Coaledo Project Revisits the Formation of the South-Central Oregon Coast" on the Geological Society of the Oregon Country website.

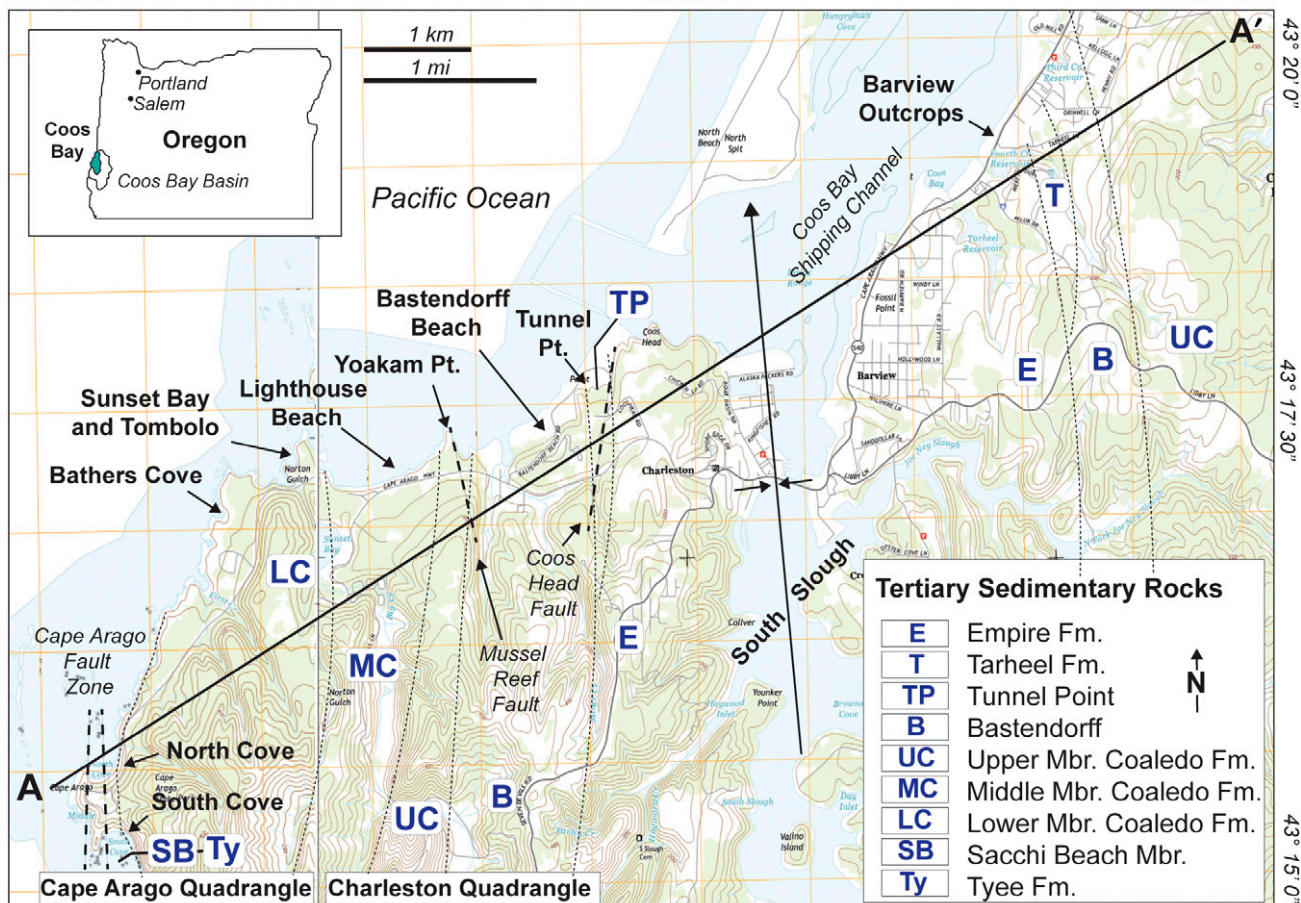


Figure 1. Geologic map of the Coos Bay area showing the rock units, South Slough plunging syncline, and location of cross section AA' of Figure 2. The Beaver Hill core hole no. 1 was drilled 10.3 km (6.4 mi) south-southeast of Cape Arago (latitude 43.240695, longitude -124.307917). Fm. = Formation; Mbr. = Member; Pt. = Point.

depositional sequences primarily featuring northward paleocurrents at present-day coordinates (Wells et al., 2014; Wells and Niem, 2021).

A change in regional tectonics during the late Oligocene (ca. 34–25? Ma) resulted in southwest-northeast compression (present-day coordinates) expressed in the Coos Bay area by the northwest-southeast-trending South Slough syncline and Coos Bay coal field fold-thrust faulting (Thompson et al., 2019). This compressive upper plate deformation, and possibly underplating, caused uplift of the southern Coast Range. This uplift propagated progressively northward, separating the forearc into subregional Neogene depocenters by right-lateral strike-slip faults and clockwise rotation driven by basin/range westward extension and San Andreas transform system northward compression (Wells et al., 2017; Darin et al., 2022).

Significant Neogene deformation events resulted in a mid-Miocene (18–30 Ma) unconformity between the Tarheel and Empire Formations, and a late Miocene–Pliocene (<7? Ma) post-Empire unconformity (Figure 3). New paleomagnetic data from the Cape Arago section suggests $\sim 70^\circ$ ($\pm 25^\circ \approx 40^\circ$ – 90° ; Blackwell et al., 2021) of post-Eocene clockwise rotation, and paleocurrents from magnetic and field indicators that imply a coastline oriented roughly southwest-northeast before tectonic rotation (Ryberg, 1978; Heller and Ryberg, 1983; Wells et al., 2014; Blackwell et al., 2021).

Coaledo Delta Development and Paleogeography

During and throughout the Eocene, active tectonism delivered volcanic detritus to the Pacific Northwest,

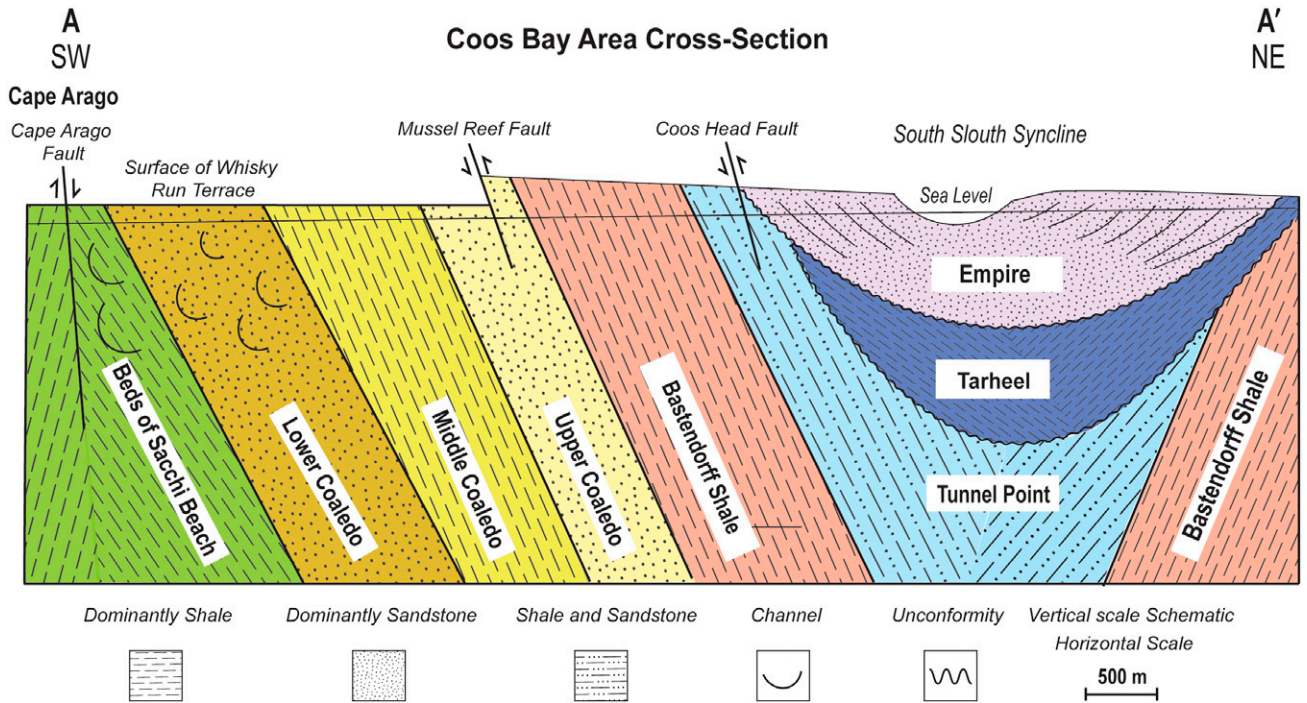


Figure 2. Geologic cross section AA' across the Coos Bay study area (see Figure 1). The Cape Arago fault marks the southwest end of the section. The Paleogene section is relatively conformably and unconformably overlaying the two unconformity-bound Neogene sequences.

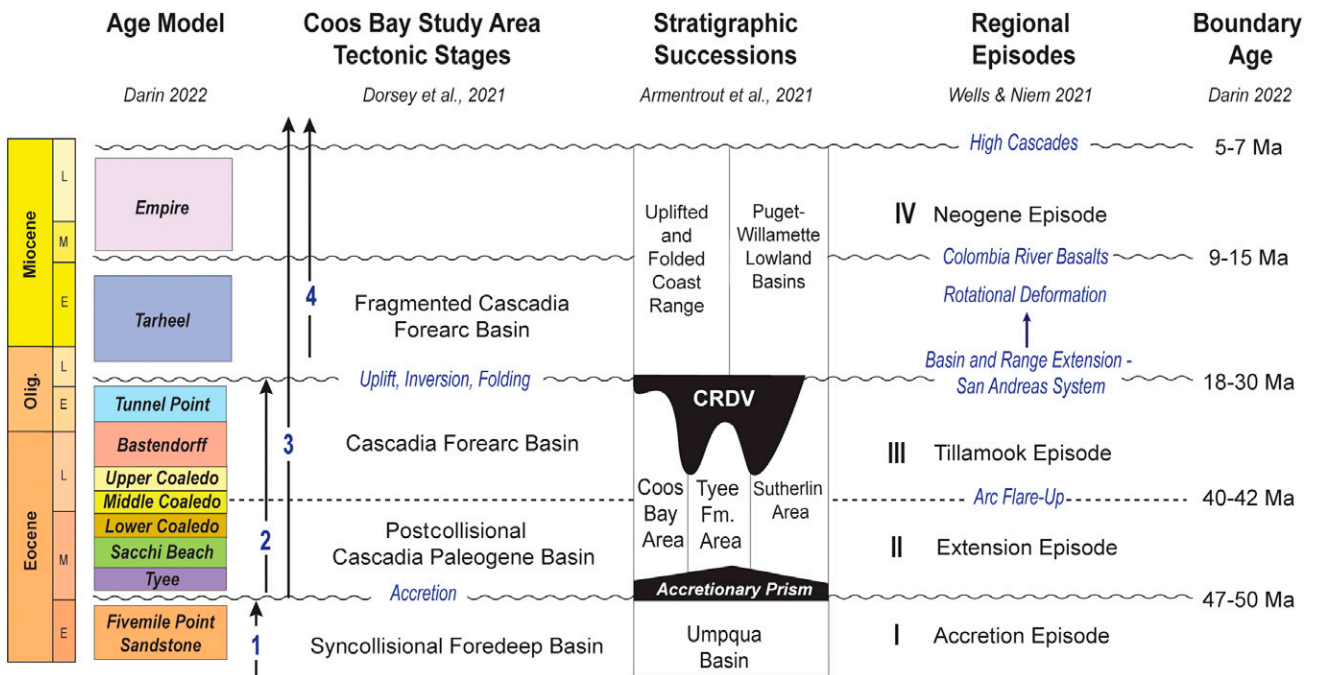


Figure 3. Correlation of tectonostratigraphic episodes and Coos Bay area tectonic stages, western Oregon and southwestern Washington. Coast Range degradational vacuity (CRDV) representing the time-space value (hiatus) differentially eroded across the southern Oregon Coast Range (after Armentrout et al., 2021). Age model and approximate age boundaries after Darin et al. (2022) and personal communication, 2023. E = early; Fm. = Formation; L = late; M = middle; Olig. = Oligocene.

B. Slope Turbidites C. Prodelta Channels D. Distributary Channels E. Prograding Shoreface

Agate Beach, Seven Devils area



North Cove, Cape Arago



Collapse Cave Point, Shore Acres



Bathers Cove, Shore Acres

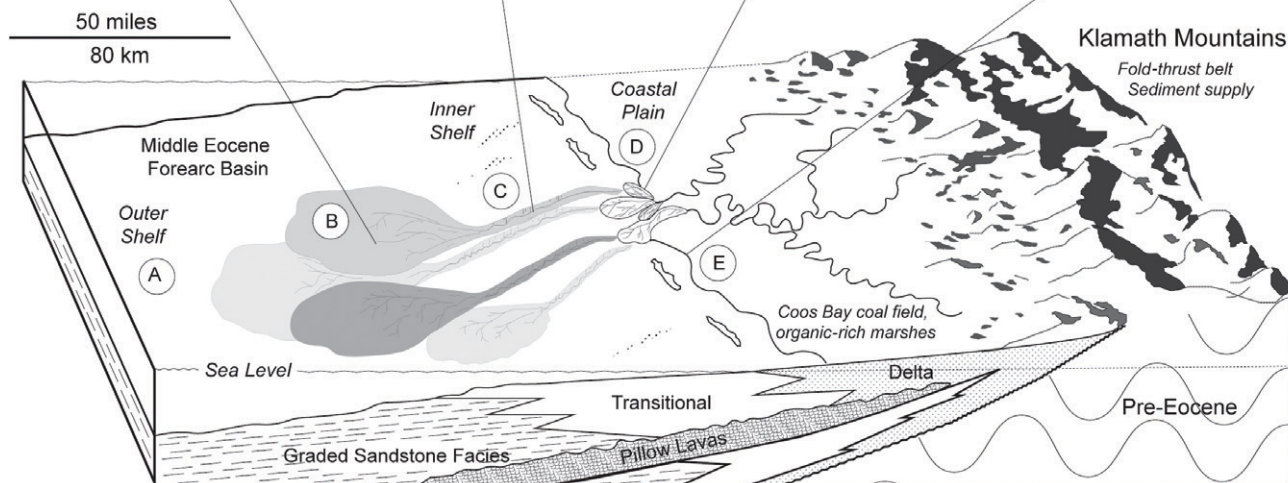


Figure 4. Proposed paleogeographic setting of several Coaledo Formation deltaic facies (modified after Dott and Bird, 1979). Photographs taken during the field seasons of 2019 and 2022. Facies A = offshore mudstone. The Agate Beach outcrop is 6.46 km (4.01 mi) south of Cape Arago (latitude 43.248913, longitude -124.388913).

where the Coaledo Delta and associated coal swamp complex is exceptionally preserved in the modern-day Coos Bay Basin (Dott, 1966; Chan and Dott, 1986). The roughly 3 km of Coaledo Delta sediments are well preserved and display sedimentary structures encompassing slope turbidites, prodelta channels, distributary channels, marsh-swamp, and prograding shoreface facies (Figure 4). The Coaledo Delta consists of two cycles of deltaic progradation and development (Lower and Upper Coaledo), in which each cycle is separated and followed by a significant transgressive sequence (Middle Coaledo and Bastendorff Shale). The lateral persistence of Coaledo deltaic outcrops is perpendicular to the northern direction of distributary channel paleocurrent indicators, suggesting that the sandstone bodies may be strike aligned due to reworking by wave processes. In addition, abundant wave-formed sedimentary structures and the relative lack of abundant tidal

structures classify the Coaledo Delta as a wave-dominated system (Chan and Dott, 1986).

Dott and Bird (1979) presented a restoration of inferred relations of middle and late Eocene lithofacies for the Coaledo Delta (Figure 4). The paleogeographic concepts are based on both regional lithofacies analysis and the outcrops along Cape Arago exposed in the cliffs of both north and south coves (Dott, 1966; Dott and Bird, 1979). The Cape Arago outcrop interpretation of progressive shallowing from upper Sacchi Beach to lowermost Coaledo Formation lithofacies assemblages supports the Dott and Bird (1979) paleogeographic model of a prograding deltaic system. Dott and Bird (1979) envisioned a broad coal-swamp coastal plain with river distributaries delivering sandy sediments from the paleo-Klamath Mountain's Canyonville fault deformation zone through prodelta channels feeding a submarine fan (Dott, 1966; Wells et al., 2000; Santra et al., 2013).

Pre-Coaledo, Sacchi Beach distal prodeltaic facies are predominately gravity flow (turbiditic), mostly centimeter-scale laminated siltstone with thin channelized and ripple-laminated fine-grained sandstone, and minor thicker turbidite sandstone beds with abundant mudstone rip-ups or intraclasts (Figure 4, labels A–C). This Sacchi Beach facies assemblage grades upward into large-scale (tens of meters) nested multistoried channel complexes. The channel-complex facies assemblage grades upward into trough cross-bedded sandstones with coarse-grained basal lags, often conglomeratic, abundant siltstone intraclasts, and coalified wood fragments, interpreted as distributary facies of the lowermost Coaledo Formation (Figure 4, labels D and E) (Dott, 1966).

Early interpretations suggested an unconformity between Sacchi Beach and Coaledo mapping units. This is based on local channel-scale intraclast conglomerates (Turner, 1938; Allen and Baldwin, 1944) and the projection of a mapped discontinuity seen farther east in deformational areas (Baldwin, 1961). Subsequent sedimentologic and biofacies interpretations along the coast from Fivemile Point near Bandon to Cape Arago support a conformable prograding-delta lithofacies progression. Discontinuities are linked to local channelization of the deltaic distributaries (Dott, 1966; Baldwin and Beaulieu, 1973; Madin et al., 1995; Wiley et al., 2015; Armentrout, 2021). In addition, previous studies by Chan and Dott (1986) and Ryberg (1978) identify up to 10 coarsening upward cycles within the Lower Coaledo.

The Lower Coaledo gradationally transitions into the Middle Coaledo, which is composed almost entirely of mudstone, claystone, and siltstone, with prominent sandstone near the top of the section. The Middle Coaledo displays laminated mudstones and turbidites, suggesting outer shelf, distal marine facies (Figure 4, labels A and B), and gradationally transitions to the Upper Coaledo. The Upper Coaledo contains thick, massive sandstone units that are cross-stratified and somewhat conglomeratic. As many as six or seven coal seams are included in the member within the Coos Bay coal field, indicating that swamps had developed after the delta sands had built up to sea level. Sandstone dikes are also prominent, but the member lacks distributary channels as found in the Lower Coaledo.

MATERIALS AND METHODS

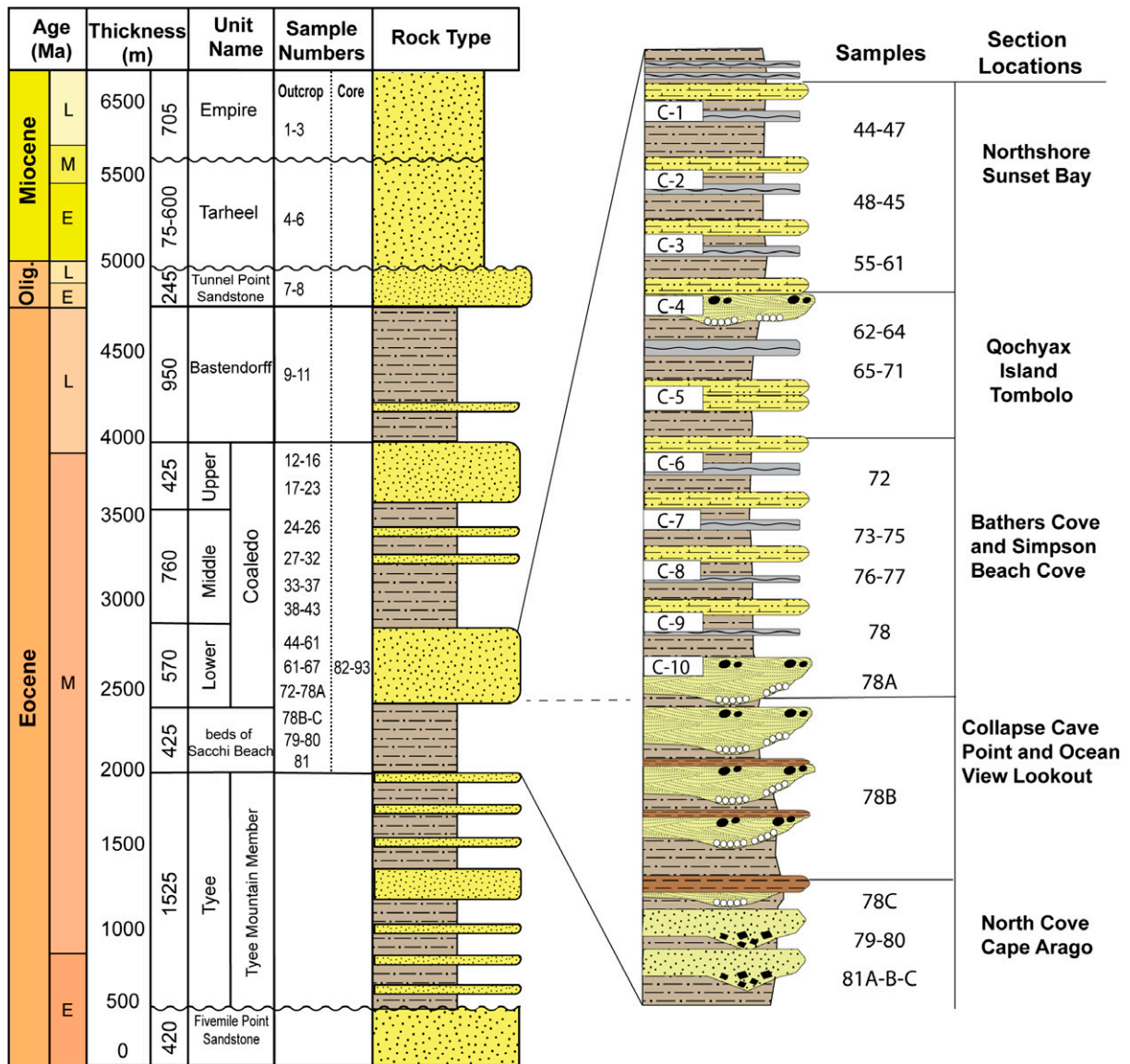
Field Sampling

To determine the geochemical and thermal maturity characteristics of the Coos Bay area, all eight rock units were sampled; they include the beds of Sacchi Beach, Coaledo (lower, middle, and upper members), Bastendorff Shale, Tunnel Point Sandstone, and Tarheel and Empire Formations. These stratigraphic unit names are those used on the most recent maps of the study area (Madin et al., 1995; Wiley et al., 2015). Samples were collected from the finest-grained lithofacies within each outcrop section. The Lower Coaledo was more densely sampled than the other units because it contains up to 10 parasequence cycles, which initially separated it as a strong candidate to produce and trap HCs effectively.

Eighty-four outcrop samples were collected from measured sections in locations along the southwest coast of Oregon: Cape Arago, Shore Acres, Sunset Bay, Lighthouse Beach, Yoakam Point, Pirates Cove, Bastendorff Beach, and Barview (Figures 1, 5). To collect samples, the weathered surface of the rock face was chipped away, and a fresh sample (~200 g) of the underlying surface was taken. Still, the effects of weathering may impact our organic geochemical data in a few ways, as described in the section Effects of Weathering. Samples were then promptly shipped to GeoMark Research in Houston, Texas, for processing. Geochemical analyses for all of the samples are inventoried in Table 1.

Core Sampling

Twelve samples were obtained from the Beaver Hill core hole no. 1 (BHC; samples 82–93), which was drilled by the Methane Energy Company in 2005 as a stratigraphic well. The core hole was drilled approximately 25 km from the Oregon coastline at a site 10.3 km southeast of Cape Arago in the center of section 12, T. 27 S., R. 14 W., in the Riverton Quadrangle, Coos County, Oregon. The core was acquired from the updip axis of the South Slough syncline, penetrating the Eocene Coaledo Formation coastal sediments (Figure 6). The core hole penetrated 1462 m (4458 ft) of the Coaledo strata with a total depth of 1368 m (4488 ft). Core descriptions by Niem et al. (unpublished report) describe the regional coastal margin



Lithologic Key

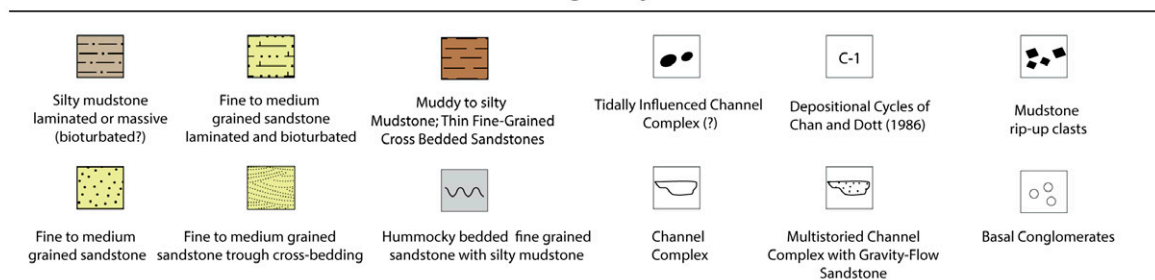


Figure 5. Generalized composite stratigraphic column for the Coos Bay area showing the relative stratigraphic position of all outcrop and core samples. Core samples 82–93 from the Beaver Hill core hole no. 1 are correlated with the Lower Coaledo Formation. Lower Coaledo sample numbers placed in the appropriate outcrop depositional cycles of Chan and Dott (1986). Corresponding sample data are shown in Table 1. Detailed sample locality information is documented in Ragan et al. (2023). E = early; L = late; M = middle; Olig. = Oligocene.

Table 1. Samples from This Study (Sample ID) and Equivalent Samples from the Ongoing US Geological Survey Microfossil Work* and Vitrinite Reflectance Work† in the Coaledo Research Project Initiative Displayed with Their Corresponding Organic Geochemistry Results from This Study

Sample ID	Field ID	USGS Microfossil No.	Rock Unit Name	Sample Type	LECO TOC, wt. %	S_{11} , mgHC/g	S_{21} , mgHC/g	S_{31} , mgCO ₂ /g	S_2/S_3	T_{max} , °C	VRE, %	Barbato et al.,		Kerogen				
												Measured %Ro	H _I , mgHC/g TOC	O _I , mgCO ₂ /g TOC	CaCO ₃ , wt. %	HAWK DM	Petrography	
1	JA-BV-12	Mf14569	Empire	Outcrop	0.22	0.2	0.2	0.67	0.30	Un.	Un.	90	302	0.50	10.35	Un.	D	III
2	JA-BV-11	Mf14568	Empire	Outcrop	0.29	0.06	0.06	0.39	0.15	Un.	Un.	21	136	0.50	6.07	Un.	D	III
3	JA-BV-9	Mf14567	Empire	Outcrop	0.13	0.07	0.06	0.34	0.18	Un.	Un.	48	270	0.54	8.64	Un.	D	III
4	JA-BV-8	Mf14566	Tarheel	Outcrop	0.29	0.08	0.08	0.46	0.17	Un.	Un.	28	159	0.50	12.33	Un.	D	III
5	JA-BV-4	Mf14562	Tarheel	Outcrop	0.26	0.06	0.08	0.43	0.19	Un.	Un.	30	163	0.43	9.66	Un.	U	III
6	JA-BV-1	Mf14559	Tarheel	Outcrop	0.33	0.07	0.11	0.62	0.18	Un.	Un.	33	186	0.39	13.01	Un.	U	III
7	"Tunnel Point"	No sample	Tunnel Point	Outcrop	0.43	0.11	0.12	0.5	0.24	Un.	Un.	28	115	0.48	12.97	Un.	U	III
8	JA (A)-TP1	No sample	Tunnel Point	Outcrop	0.48	0.04	0.12	0.5	0.24	Un.	Un.	25	105	0.25	13.97	Un.	D/U	III
9	JA (A)-BAS2	No sample	Bastendorff	Outcrop	1.27	0.09	1.01	0.88	1.15	412	0.256	80	69	0.08	13.90	III	D	III
10	JA(A)-BAS1	No sample	Bastendorff	Outcrop	0.89	0.1	0.55	1.25	0.44	420	0.4	62	140	0.15	14.72	III	D	III
11	"Bastendorff"	No sample	Bastendorff	Outcrop	1.39	0.08	1.12	1.46	0.77	420	0.4	81	105	0.07	13.60	III	III	III
12	JA-YPC-3	Mf14588	Upper Coaledo	Outcrop	0.83	0.03	0.33	0.94	0.35	435	0.67	40	114	0.08	11.30	III	III	III
13	JA-A-6	Mf14553	Upper Coaledo	Outcrop	0.50	0.04	0.2	0.53	0.38	437	0.706	40	105	0.17	12.80	III	D	III
14	JA-A-5	Mf14552	Upper Coaledo	Outcrop	1.00	0.08	0.36	1.23	0.29	435	0.67	36	123	0.18	16.25	III	III	III
15	JA-YPC-2	Mf14557	Upper Coaledo	Outcrop	0.74	0.06	0.24	1.08	0.22	431	0.598	32	146	0.20	16.29	III	III	III
16	JA(A)-4	No sample	Upper Coaledo	Outcrop	0.28	0.05	0.08	0.86	0.09	Un.	Un.	29	308	0.39	19.59	Un.	III	III
17	JA-YPC-1	Mf14556	Upper Coaledo	Outcrop	0.04	0.02	0.04	0.24	0.17	Un.	Un.	111	665	0.33	16.45	Un.	III	III
18	JA-YPS-8	Mf14555	Upper Coaledo	Outcrop	1.06	0.11	0.94	1	0.94	421	0.418	89	94	0.11	15.90	III	D	III
19	JA-YPS-7	Mf14547	Upper Coaledo	Outcrop	5.00	0.12	2.96	2.17	1.36	419	0.382	59	43	0.04	15.34	III	D	III
19A	JA-YPBHC-1	No sample	Upper Coaledo	Outcrop	52.30	0.77	67.65	21.21	3.19	421	0.418	129	41	0.01	15.15	III	III	III
20	JA-YPS-6	Mf14553	Upper Coaledo	Outcrop	0.13	0.09	0.04	0.35	0.11	Un.	Un.	32	278	0.69	19.89	III	D	III
21	JA-YPS-4	Mf14551	Upper Coaledo	Outcrop	0.93	0.03	0.34	0.87	0.39	432	0.616	37	94	0.08	14.97	III	III	III
22	JA-YPS-2	Mf14549	Upper Coaledo	Outcrop	1.44	0.06	0.71	1.26	0.56	438	0.724	49	88	0.08	15.73	III	D	III
23	JA-LH-54	Mf14547	Middle Coaledo	Outcrop	0.24	0.07	0.15	0.42	0.36	Un.	Un.	63	176	0.32	16.27	Un.	III	III
24	JA-LH-51	Mf14544	Middle Coaledo	Outcrop	1.34	0.07	0.88	1.19	0.74	431	0.598	66	89	0.07	17.86	III	III	III
25	JA-LH-49	Mf14542	Middle Coaledo	Outcrop	1.32	0.1	1.11	1.14	0.97	428	0.544	84	86	0.08	16.57	III	III	III
26	JA-LH-45	Mf14538	Middle Coaledo	Outcrop	1.97	0.1	2.89	0.81	3.57	428	0.544	147	41	0.03	18.53	III	D	III
27	JA-LH-41	Mf14533	Middle Coaledo	Outcrop	0.75	0.07	0.4	0.88	0.45	433	0.634	54	118	0.15	13.95	III	III	III
28	JA-LH-34	Mf14526	Middle Coaledo	Outcrop	1.10	0.06	0.66	0.76	0.87	433	0.634	60	69	0.08	14.16	III	D	III
29	JA(A)-1H	No sample	Middle Coaledo	Outcrop	4.07	0.12	1.84	1.13	1.63	427	0.526	45	28	0.06	14.99	III	D	III
30	JA(A)-LH-2	No sample	Middle Coaledo	Outcrop	0.86	0.08	0.51	0.78	0.65	428	0.544	60	91	0.14	12.50	III	III	III
31	JA-LH-1	No sample	Middle Coaledo	Outcrop	0.37	0.06	0.27	0.42	0.64	428	0.544	73	14	0.18	10.38	III	D	III
33	JA-LH-26	Mf14516	Middle Coaledo	Outcrop	2.26	0.14	7.14	0.99	7.21	421	0.418	316	44	0.02	16.04	III	III	III
34	JA-LH-23	Mf14511	Middle Coaledo	Outcrop	1.83	0.11	5.17	0.82	6.30	419	0.382	283	45	0.02	17.70	III	III	III
36	JA-LH-16	Mf14503	Middle Coaledo	Outcrop	0.90	0.1	1.56	0.63	2.48	426	0.508	173	70	0.06	13.52	III	III	III
37	JA-LH-11	Mf14497	Middle Coaledo	Outcrop	1.23	0.08	1.06	0.45	2.36	428	0.544	86	37	0.07	17.15	III	D	III
38	JA-SSB-10	Mf14486	Middle Coaledo	Outcrop	1.28	0.06	0.43	0.92	0.47	431	0.598	34	72	0.12	15.72	III	III	III
39	JA-SSB-5	Mf14481	Middle Coaledo	Outcrop	0.85	0.04	0.36	0.61	0.59	432	0.616	42	72	0.10	13.93	III	III	III

(continued)

Table 1. Continued

Sample ID	Field ID	USGS Microfossil No.	Rock Unit Name	Sample Type	LECO TOC, wt. %	S_{11} , mgHC/g	S_{21} , mgHC/g	S_{31} , mgCO ₂ /g	S_2/S_3	T_{max} , °C	VRE, %	Barbato et al., Measured %R ₀	H_I , mgHC/g TOC	O_I , mgCO ₂ /g TOC	Kerogen		
															CaCO ₃ , wt. %	PI	Petrography
40	JA-SSB-3	MF14479	Middle Coaledo	Outcrop	1.09	0.04	0.47	0.74	0.64	435	0.67		43	68	14.48	III	
41	JA-SSB-1	MF14477	Middle Coaledo	Outcrop	0.34	0.04	0.13	0.6	0.22	Un.	Un.		38	177	13.89	Un.	
42	JA-MC-2	MF14476	Middle Coaledo	Outcrop	0.64	0.05	0.46	0.46	1.00	431	0.598		72	72	13.72	III	
43	JA-MC-1	MF14475	Middle Coaledo	Outcrop	1.11	0.04	0.54	0.7	0.77	427	0.526		49	63	13.75	III	
44	JA-CB-4	MF14471	Lower Coaledo	Outcrop	1.54	0.09	1.11	0.99	1.12	439	0.742		72	64	14.2	III U	
45	JA-CB-3	MF14474	Lower Coaledo	Outcrop	0.28	0.04	0.13	0.36	0.36	Un.	Un.	0.391	47	130	13.16	III U	
46	JA-CB-2	MF14473	Lower Coaledo	Outcrop	0.77	0.09	0.28	0.44	0.64	434	0.652	0.413	36	57	14.75	III D	
47	JA-CB-1	MF14472	Lower Coaledo	Outcrop	0.93	0.08	0.43	0.85	0.51	432	0.616		46	91	14.00	III	
47A	JA-Sunbay-1	No sample	Lower Coaledo	Outcrop	0.98	0.03	0.76	0.3	2.53	436	0.688		78	31	10.66	III	
48	JA(A)-B6	No sample	Lower Coaledo	Outcrop	1.15	0.08	0.89	0.95	0.94	438	0.724		77	83	12.33	III	
49	JA-B-5	MF14443	Lower Coaledo	Outcrop	0.61	0.03	0.31	0.56	0.55	434	0.652		51	92	15.01	III	
50	JA-B-4	MF14435	Lower Coaledo	Outcrop	0.90	0.08	0.45	0.66	0.68	433	0.634		50	73	14.77	III D	
51	JA-B-3	MF13429	Lower Coaledo	Outcrop	1.03	0.04	0.56	0.95	0.59	435	0.67		54	92	14.12	III	
52	JA(A)-B-1B	No sample	Lower Coaledo	Outcrop	1.50	0.02	0.58	0.75	0.77	430	0.58		39	50	11.84	III	
53	JA-B-2	MF14419	Lower Coaledo	Outcrop	0.72	0.06	0.38	0.4	0.95	425	0.49		53	56	15.51	III D	
54	JA(A)-B-1A	No sample	Lower Coaledo	Outcrop	0.68	0.06	0.33	0.86	0.38	427	0.526		49	127	17.11	III	
55	JA-B-B1	MF14403	Lower Coaledo	Outcrop	0.53	0.02	0.22	0.54	0.41	433	0.634		42	102	15.94	III	
56	JA(A)-A-6	No sample	Lower Coaledo	Outcrop	0.79	0.07	0.51	0.54	0.94	436	0.688		64	68	9.10	III	
57	JA-A-5	MF14389	Lower Coaledo	Outcrop	2.18	0.04	1.81	1.23	1.47	439	0.742		83	56	9.47	III	
58	JA-A-4	MF14384	Lower Coaledo	Outcrop	0.71	0.03	0.42	0.72	0.58	436	0.688		59	101	15.40	III	
59	JA-A-3	MF14383	Lower Coaledo	Outcrop	0.18	0.02	0.07	0.47	0.15	Un.	Un.		38	255	38.93	Un.	
60	JA-A-2	MF14382	Lower Coaledo	Outcrop	1.09	0.08	0.46	0.68	0.68	435	0.67	0.477	42	62	15.79	III D	
61	JA-A-1	MF14381	Lower Coaledo	Outcrop	1.14	0.04	0.53	0.93	0.57	434	0.652		46	82	14.05	III	
62	JA-QIT-25	MF14380	Lower Coaledo	Outcrop	1.44	0.06	1.09	0.75	1.45	437	0.706		76	52	10.77	III	
63	JA-QIT-21	MF14376	Lower Coaledo	Outcrop	0.91	0.06	0.46	0.82	0.56	432	0.616		50	90	11.32	III	
64	JA-QIT-18	MF14373	Lower Coaledo	Outcrop	0.69	0.09	0.39	0.62	0.63	434	0.652		57	90	9.20	III	
65	JA-QIT-16	MF14371	Lower Coaledo	Outcrop	1.44	0.05	0.86	0.96	0.90	435	0.67		60	67	7.50	III	
66	JA-QIT-14	MF14369	Lower Coaledo	Outcrop	0.92	0.09	0.74	1.02	0.73	432	0.616		81	111	9.89	III	
67	JA-QIT-10	MF14365	Lower Coaledo	Outcrop	0.98	0.07	0.87	0.64	1.36	430	0.58		89	65	13.06	III	
68	JA-QIT-7	MF14362	Lower Coaledo	Outcrop	0.59	0.05	0.27	0.61	0.44	425	0.49		45	103	9.64	III	
69	JA-QIT-6	MF14361	Lower Coaledo	Outcrop	0.80	0.05	0.35	0.6	0.58	425	0.49		44	75	9.46	III	
71	JA-QIT-2	MF14357	Lower Coaledo	Outcrop	0.47	0.09	0.25	0.45	0.56	436	0.688		54	97	0.27	6.38	
72	JA-SABC-12	MF14355	Lower Coaledo	Outcrop	1.04	0.03	0.9	0.7	1.29	437	0.706		87	67	7.87	III	
73	JA-SABC-10	MF14353	Lower Coaledo	Outcrop	0.68	0.07	0.37	0.59	0.63	429	0.562		54	86	16.60	III U	
75	JA-SABC-6	MF14345	Lower Coaledo	Outcrop	0.74	0.11	0.39	0.47	0.83	432	0.616		53	64	15.28	III D	
76	JA-SABC-4	MF14343	Lower Coaledo	Outcrop	0.32	0.05	0.19	0.36	0.53	428	0.544		60	113	13.39	III	
77	JA(A)-7	No sample	Lower Coaledo	Outcrop	0.99	0.04	1.05	0.62	1.69	431	0.598		106	63	17.20	III	
78	JA-OBC-1	No sample	Lower Coaledo	Outcrop	0.33	0.1	0.16	0.37	0.43	432	0.616	0.697	48	111	13.68	III	
78A	JA-PS5-1	No sample	Lower Coaledo	Outcrop	0.78	0.04	0.46	0.31	1.48	440	0.76		59	40	11.49	III D	

(continued)

Table 1. Continued

Sample ID	Field ID	USGS Microfossil No.	Rock Unit Name	Sample Type	LECO TOC, wt. %	S_{11} , mgHC/g	S_{21} , mgHC/g	S_{22} , mgCO ₂ /g	S_{23} , mgCO ₂ /g	T_{max} , °C	VRE, %	Barbato et al., Measured %aR ₀	H_{II} , mgHC/g TOC	O_{II} , mgCO ₂ /g TOC	Kerogen		
															PI	HAWK	DM Petrography
78B	JA-PS3-1	No sample	Lower Coaledo	Outcrop	1.34	0.07	1.17	0.33	3.55	439	0.742		87	25	0.06	8.40	III
78C	JA-SB-1	No sample	Sacchi Beach	Outcrop	0.86	0.04	0.53	0.26	2.04	441	0.778		62	30	0.07	9.70	III
79	JA-NCCA-11	Mf14291	Sacchi Beach	Outcrop	0.72	0.06	0.59	0.76	0.78	436	0.688		82	105	0.09	11.60	III
80	JA-NCCA-12	Mf14288	Sacchi Beach	Outcrop	1.02	0.09	1.05	0.45	2.33	434	0.652	0.408	103	44	0.08	13.46	III D
81A	JA-SB-2	No sample	Sacchi Beach	Outcrop	0.72	0.02	0.54	0.37	1.46	437	0.706		75	51	0.04	7.36	III
81B	JA-SB-3	No sample	Sacchi Beach	Outcrop	0.91	0.04	0.85	0.33	2.58	436	0.688		94	36	0.04	11.22	III
81C	JA-SB-4	No sample	Sacchi Beach	Outcrop	1.51	0.03	1.67	0.35	4.77	439	0.742		111	23	0.02	9.67	III
82	BHC 3874.5	No sample	Lower Coaledo	Core	48.60	1.73	139.18	17.56	7.93	417	0.346	0.318	286	36	0.01	6.46	II U
83	BHC 4003.5	No sample	Lower Coaledo	Core	1.99	0.07	2.05	1.64	1.25	435	0.67		103	82	0.03	16.54	III D
84	BHC 4033.8	No sample	Lower Coaledo	Core	10.20	0.2	30.89	2.01	15.37	428	0.544	0.364	303	20	0.01	10.28	II L
85	BHC 4092.5	No sample	Lower Coaledo	Core	12.50	0.29	20.73	7.06	2.94	420	0.4		166	56	0.01	6.48	II U
86	BHC 4133.2	No sample	Lower Coaledo	Core	31.00	0.49	29.69	10.82	2.74	413	0.274		96	35	0.02	16.29	III U
87	BHC 4215	No sample	Lower Coaledo	Core	13.40	0.56	14.96	6.45	2.32	408	0.184	0.365	112	48	0.04	26.63	III D
88	BHC 4245.5	No sample	Lower Coaledo	Core	7.95	0.31	12.48	3.02	4.13	412	0.256		157	38	0.02	13.46	III D
89	BHC 4249.5	No sample	Lower Coaledo	Core	2.26	0.12	3.56	1.27	2.80	424	0.472		158	56	0.03	7.00	III D
90	BHC 4345.5	No sample	Lower Coaledo	Core	16.40	0.89	32.56	7.06	4.61	412	0.256		199	43	0.03	19.70	III D
91	BHC 4394	No sample	Lower Coaledo	Core	0.23	0.04	0.21	0.38	0.55	432	0.616		93	167	0.16	12.73	III D
92	BHC 4394.5	No sample	Lower Coaledo	Core	9.51	0.37	13.91	4.15	3.35	417	0.346	0.401	146	44	0.03	16.67	III A
93	BHC 4457	No sample	Lower Coaledo	Core	2.06	0.06	1.56	1.08	1.44	440	0.76	0.344	76	52	0.04	14.33	III D

Samples removed for their poor remaining generative potential (S_2) peak development and their associated thermal maturity (T_{max}) and vitrinite reflectance equivalent (VRE) are marked "Un," for unreliable data. HAWK pyrolysis data: free hydrocarbon (S_1), S_2 , and trapped CO_2 , S_3 ; calculated VRE, hydrogen index (HI), oxygen index (OI), production index (PI), T_{max} , and HAWK. Organic petrography data: dominant maceral (DM), where D = detrohuminite; U = ulminite B; L = liptodetrinite, and A = atrinite. Kerogen (petrography) signifies the kerogen type of the sample determined via organic petrography on 40 select samples. Beaver Hill core hole no. 1 (BHC) (depth in feet); samples from the BHC are Lower Coaledo, with increasing depth from samples 82 to 93.

Abbreviations: ID = identifier; USGS = US Geological Survey.

*Ragan et al. (2023).

†Barbato et al., data not shown.

setting of the Lower Coaledo interval (527 m [1728 ft]), marine transgression of the Middle Coaledo (750 m [2460 ft]), and regression of coastal plain to shoreface facies in the Upper Coaledo (186 m [609 ft]).

Indications of interbedded marine facies were substantiated by rare molluscan fossils and neritic foraminifera recovered from thin mudstone (D. McKeel, consultant's report, 2005, cited by Niem et al., unpublished report). Samples were taken from the Lower Coaledo section of the core from carbonaceous shale intervals that were near coal layers or contained coaly fragments (Figure 6). The 12 core samples from the lower member of the Coaledo Formation, plus the 84 outcrop samples, bring the total sample inventory to 96 (Table 1).

Effects of Weathering

In this study, both outcrop and core samples have been evaluated for their source rock geochemistry. It is important to note that outcrop samples and equivalent

core samples will likely display different intensities of geochemical signatures due to overprinting caused by weathering. Over time, physical and chemical weathering of the outcrop alters the integrity of the rock and causes changes to the original organic geochemical signature of a sample, which is better preserved in the subsurface. When weathering takes place, pyrolysis source rock indicators can be affected in several ways (Dembicki, 2017). First, outcrops tend to have lower free hydrocarbon (S_1) values because the free HCs are more easily oxidized compared to subsurface core samples. Second, the remaining organic matter (S_2) can weather out of the rock and/or be oxidized, especially in higher porosity rock formations. Combined, these scenarios make the sediment appear less organic rich, or display a lower TOC weight percent, than it may actually be in the subsurface (Law et al., 1984). Since oxidation of source material can affect the S_2 of a sample, its T_{max} may also be affected, making the sample appear more mature and more gas prone than oil prone (Dembicki, 2017). Weathering can be

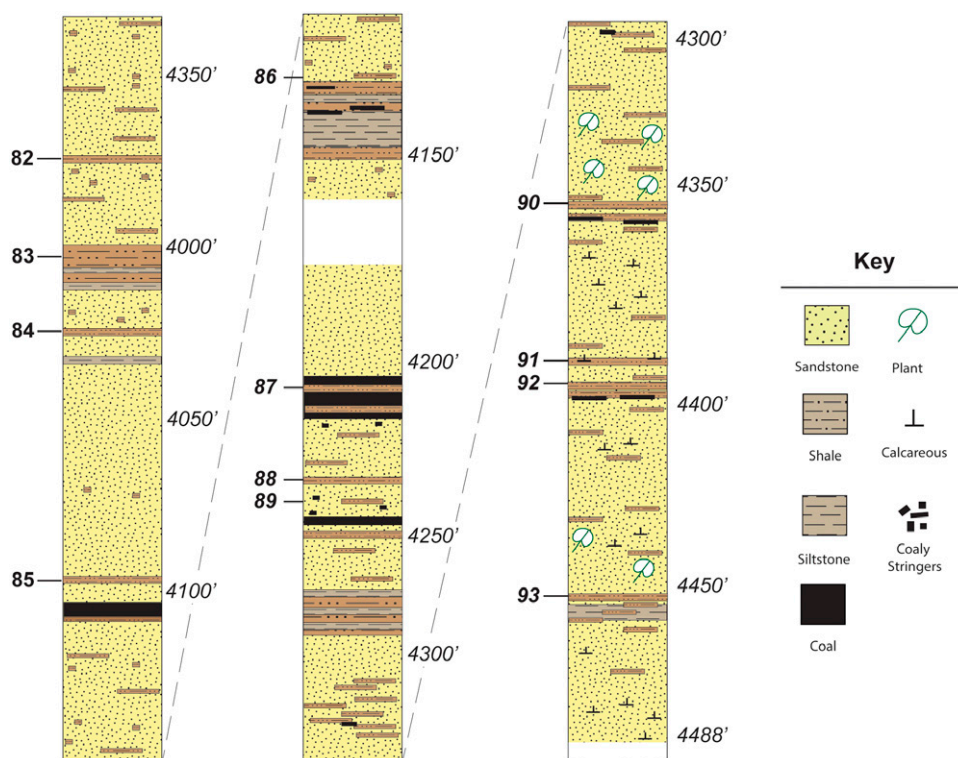


Figure 6. Lithology for the Lower Coaledo Formation and samples collected from the Beaver Hill core hole no. 1. Corresponding depths are noted in Table 1. Three coal seams shown in this log indicate that both the Lower Coaledo Formation and the extensively mined Upper Coaledo contain coal seams in the coastal plain facies of the Coos Bay coal field. Reproduced with permission from Methane Energy Corporation.

inconsistent across an area; however, for this study, it was assumed that weathering was proportional across outcrop samples given the relatively small extent of our sampled area along the Oregon coast and for the core samples to exhibit clear geochemical responses. Differences between outcrop and core S_1 and S_2 are considered in the Results and the Discussion sections.

TOC

Approximately 200 mg of sample material was used for TOC analysis using a LECO C230 instrument. Samples were weighed and ground into a homogeneous powder using a mortar and pestle until they passed through a 60-mesh sieve. Samples were then treated with concentrated hydrochloric acid for at least 2 hr to remove any inorganic carbon. The remaining sample material was rinsed with water and flushed through a filtration apparatus to remove the acid. The filter was then removed, placed into a LECO crucible, and dried in a low-temperature oven (110°C) for a minimum of 4 hr. Samples were weighed after this process to obtain a percent carbonate value based upon loss from the original measured weight. The LECO instrument was calibrated against a set of standards of known carbon content. The sample and standard material were combusted at 1200°C in the presence of oxygen, with the resulting carbon being converted to carbon dioxide and measured on an infrared cell. Standards were analyzed as unknowns every 10 samples to check the variation and calibration of the analysis. Random and selected reruns were done to quality assurance/quality control the measured data. The acceptable standard deviation for TOC is $\pm 3\%$ variation from the established value.

HAWK Pyrolysis

During HAWK pyrolysis, roughly 70 mg of washed, ground samples were subjected to stages of gradual heating in an inert helium atmosphere. As temperature increased and samples thermally decomposed, organic compounds generated from the samples were quantitatively measured by a flame ionization detector (FID), and relative abundances of the produced gases over time were displayed as peaks (S_1 , S_2 , and trapped CO_2 [S_3]) on a pyrogram (Peters and Cassa, 1994; Carvajal-Ortiz and Gentzis, 2015; Dembicki, 2017).

During the first stage of pyrolysis, the samples were heated to 300°C, where the temperature was held for 3 min. Volatile organic material released from the sample during this stage was measured in mg HC/g of rock and is referred to as the S_1 peak. The S_1 values represent so-called free HCs that have already been released from the sample's kerogen due to natural thermal maturation processes over the course of geologic time. The temperature was then increased again from 300°C to 650°C at a rate of 25°C/min, and the volatile organic gases measured by the FID constitute the S_2 , which is also measured in mg HC/g of rock. The S_2 peak represents the HC-generating potential remaining in the sediment's kerogen that was not previously broken down during natural heating through geologic processes. The temperature at which the S_2 peak reaches its apex is recorded as the T_{max} (Espitalié, 1986; Peters, 1986; Dembicki, 2017). The T_{max} results were filtered based upon an S_2 threshold value and on the morphology of the S_2 peak in the pyrogram, selection criteria that are discussed further in the following section. Lastly, the CO_2 released and trapped between 300°C and 400°C is referred to as the S_3 peak and is measured in mg CO_2 /g of rock (Espitalié, 1986; Peters, 1986).

The LECO-derived TOC weight percent is used in combination with the S_1 , S_2 , and S_3 values to provide additional information on a sample's organic geochemical characteristics such as the kerogen type, HI, oxygen index (OI), and production index (PI), results shown in Table 1. A calculated vitrinite reflectance equivalent (VRE) is also reported from the HAWK-derived T_{max} value, and it is calculated using the Jarvie 2001 equation (Jarvie et al., 2001).

$$\begin{aligned} HI &= S_2/TOC \times 100 \text{ (reported in mg HC/g TOC)} \\ OI &= S_3/TOC \times 100 \text{ (reported in mg CO}_2\text{/g TOC)} \\ PI &= S_1/(S_1 + S_2) \\ VRE &= (0.018 \times T_{max}) - 7.16 \end{aligned} \quad (1)$$

Although the Jarvie 2001 equation is used, it is important to note that there are many other vitrinite reflectance, measured in percent ($\%R_o$) equivalent calculations, all of which have limitations because they are based on specific basins, with varying organofacies characteristics, and different geologic contexts (Katz and Lin, 2021). Therefore, the calculated

VRE presented in this study is a relative value, and not to be taken as an absolute.

Pyrogram Filtering

Accurate T_{max} measurements are derived from pyrograms in which the S_2 peak displays sufficient unimodality (Carvajal-Ortiz and Gentzis, 2015; Dembicki, 2017). However, if a sample fails to contain enough organic material to be pyrolyzed or contains sufficient variations in organic matter chemistry, then this can result in poor development of the S_2 peak, leading to a potentially erroneous T_{max} measurement from an inaccurately identified S_2 apex (Espitalié, 1986; Dembicki, 2017). To avoid including potentially erroneous measurements, studies suggest S_2 thresholds that are sufficiently high to avoid the possibility of including inaccurate T_{max} measurements, such as S_2 approaching 1 mg HC/g rock (Katz and Lin, 2021) or $S_2 > 0.2$ mg HC/g rock (Peters, 1986; Dembicki, 2017). However, the same studies also note that, ideally, the interpretation of the validity of T_{max} should be a multifaceted approach where possible and include an examination of the pyrograms in combination with the S_2 value. For our study, all of the T_{max} results were individually filtered based upon a hierarchical approach, beginning with a detailed evaluation of the morphology of the S_2 peaks. Peak morphology was consistently evaluated based upon the following statistical verbiage: bimodal, skewness, negative kurtosis, and unimodality. Peak filtering then roughly corresponds to an S_2 of 0.15 mg HC/g rock.

Pellet Sample Preparation

Sample pellets used for organic petrography analyses were prepared with the Kentucky Geological Survey according to the ASTM D2797 (ASTM, 2015) procedure. Approximately 30 g of each sample was air dried at 40°C, crushed to -18 mesh (<1 mm), and split with a sample riffler where necessary. The samples were mixed with an epoxy and poured into a 1-in. diameter ring mold. The sample + epoxy mixtures were left to cure for 6 to 8 hr. After curing, the samples were placed in a drying oven at 40°C. Samples were secured into the holder and ground using 320-, 4000-, and 6000-grit surfaces. After grinding, the pellets were polished with 1.0 and 0.3 μm

alumina slurries. The samples were given a final polish with 0.4 μm colloidal silica and rinsed with distilled water. Pellet surfaces were dried with compressed air and placed in a desiccator for 8 to 12 hr.

Organic Petrography: Macerals and Kerogen

Organic petrography was used alongside HI ranges to establish the kerogen type for each of the eight rock units. The kerogen type was determined by counting the maceral components of 40 samples, encompassing each of the Coos Bay rock units. The polished pellets were examined under reflected light using a petrographic microscope to acquire 100 maceral measurements. The results are shown in Table 1. Typically, biostratigraphic techniques are accurate in determining kerogen type because they provide high-resolution results, but organic petrography is also considered an informative method for kerogen typing, especially when paired with HAWK pyrolysis results.

Forty samples were investigated in white and ultraviolet (UV) light using a Zeiss Axio-Scope A1 at 500 \times in immersion oil. White and UV light were provided by an X-Cite 120 light-emitting diode light source. For each of the samples, 100 counts of macerals and associated mineral matter are collected. To identify macerals, each pellet is scanned under both white and UV light using an automated point counter (and proprietary software) attached to the stage of the microscope, where each random individual field of view was investigated under both white and UV light to reveal fluorescing liptinite macerals.

Macerals are identified using standard definitions for vitrinite (Sýkorová et al., 2005), inertinite (International Committee for Coal and Organic Petrology, 2001), and liptinite (Taylor et al., 1998; Pickel et al., 2017) for low-rank coal. Identifications and classification of mineral matter were limited to quartz, clay, carbonate, and pyrite (or other sulfide) minerals.

RESULTS

Table 1 presents a high-resolution summary of the organic geochemical variations between the eight rock units sampled at Coos Bay. Table 1 includes HAWK pyrolysis geochemistry and organic petrography results,

plus an additional column showing % R_o results from equivalent samples in Barbato et al. (data not shown). While filtering pyrograms for accurate S_2 measurements for T_{max} , 15 samples were removed, so their T_{max} and VRE values were not reported; they are described in the section Pyrograms. Their S_2 , yield, however, is still considered reliable; therefore, S_2 , HI , and PI values are presented in Table 1 for the aforementioned 15 samples. Table 2 provides the minimum, maximum, mean TOC (wt. %), and HI (mg HC/g TOC) values for each rock unit to discern broader geochemical trends between each unit, relative to changes in depositional environments over geologic time.

In general, the samples evaluated are type III kerogen (gas prone) (Figures 7–9) and low maturity (Figures 7–10) and have TOC ranges from poor to excellent. Elevated TOC values occur in the mudstones of Sacchi Beach, the Lower, Middle, and Upper Coaledo, and the Bastendorff Shale. Elevated HI values occur in the more laminated, less bioturbated facies of the Sacchi Beach and Middle Coaledo facies (see Figure 12). The Empire, Tarheel, and Tunnel Point strata are sandstones with only slightly silty intervals, so they do not contain ample organic material suitable for geochemical analysis. Differences between core and outcrop geochemistry are reflected in the S_1 and S_2 values (Table 3).

Results from the source rock geochemistry analyses are described based on their richness, quality, potential, and maturity.

Source Rock Richness

Source rock richness is evaluated from a sample's TOC weight percent. The TOC weight percent richness values are based on the terminology used by Peters and Cassa (1994): poor (0–0.5 wt. %), fair (0.5–1 wt. %), good (1–2 wt. %), very good (2–4 wt. %), and excellent (>4 wt. %). Any TOC values of ≥ 50 wt. % are coal. Lewan (1987) conducted hydrous pyrolysis experiments and found that at least 2.5 wt. % TOC was needed to create a continuous network of organic matter to be a viable, oil-prone source rock. However, gas movement from a source rock is facilitated by its movement across multiple scales (Akkutlu and Fathi, 2012). Shale gas transport predominantly relies on gas diffusion (Ziarani and Aguilera, 2011), whereas naturally fractured coals, featuring both matrix pores and fissure pores (cleats), demonstrate multicomponent gas flow via diffusion, desorption, and gas flow through cleat networks (Gao et al., 2022). The comparative ease of gas mobility to oil mobility implies that gas source material does not require as continuous an organic matter network to be considered viable. Therefore, since gas has already been encountered in Coos Bay strata, in this study, we instead use 2.0 wt. % TOC , in combination with an HI between 50 and 200 mg HC/g TOC , as the threshold for a viable gas-prone source rock.

Few outcrop samples in this data set equal or exceed 2.0 wt. % (Figure 7; Table 1); these are samples 19 and 19A in the Upper Coaledo, samples 29

Table 2. Ranges and Average Total Organic Carbon* and Hydrogen Index† from Each Rock Unit in the Coos Bay Area and the Beaver Hill Core Hole Number 1

Rock Unit	Type	No. of Samples	TOC , wt. %			HI , mg HC/g TOC		
			Min	Mean	Max	Min	Mean	Max
Empire	Outcrop	3	0.13	0.21	0.29	21	53	90
Tarheel	Outcrop	3	0.26	0.29	0.33	28	30	33
Tunnel Point	Outcrop	2	0.43	0.45	0.48	25	27	28
Bastendorff	Outcrop	3	0.89	1.18	1.39	62	74	81
Upper Coaledo	Outcrop	12	0.04	5.35	52.3	29	57	129
Middle Coaledo	Outcrop	19	0.24	1.24	4.07	34	94	316
Lower Coaledo	Outcrop	36	0.18	0.89	2.18	36	59	106
Lower Coaledo	Core	12	0.23	13.01	48.6	76	158	303
Sacchi Beach	Outcrop	6	0.72	0.96	1.51	62	88	111

Abbreviations: HI = hydrogen index; Max = maximum; Min = minimum; No. = number; TOC = total organic carbon.

*Weight percent (richness).

†Quality.

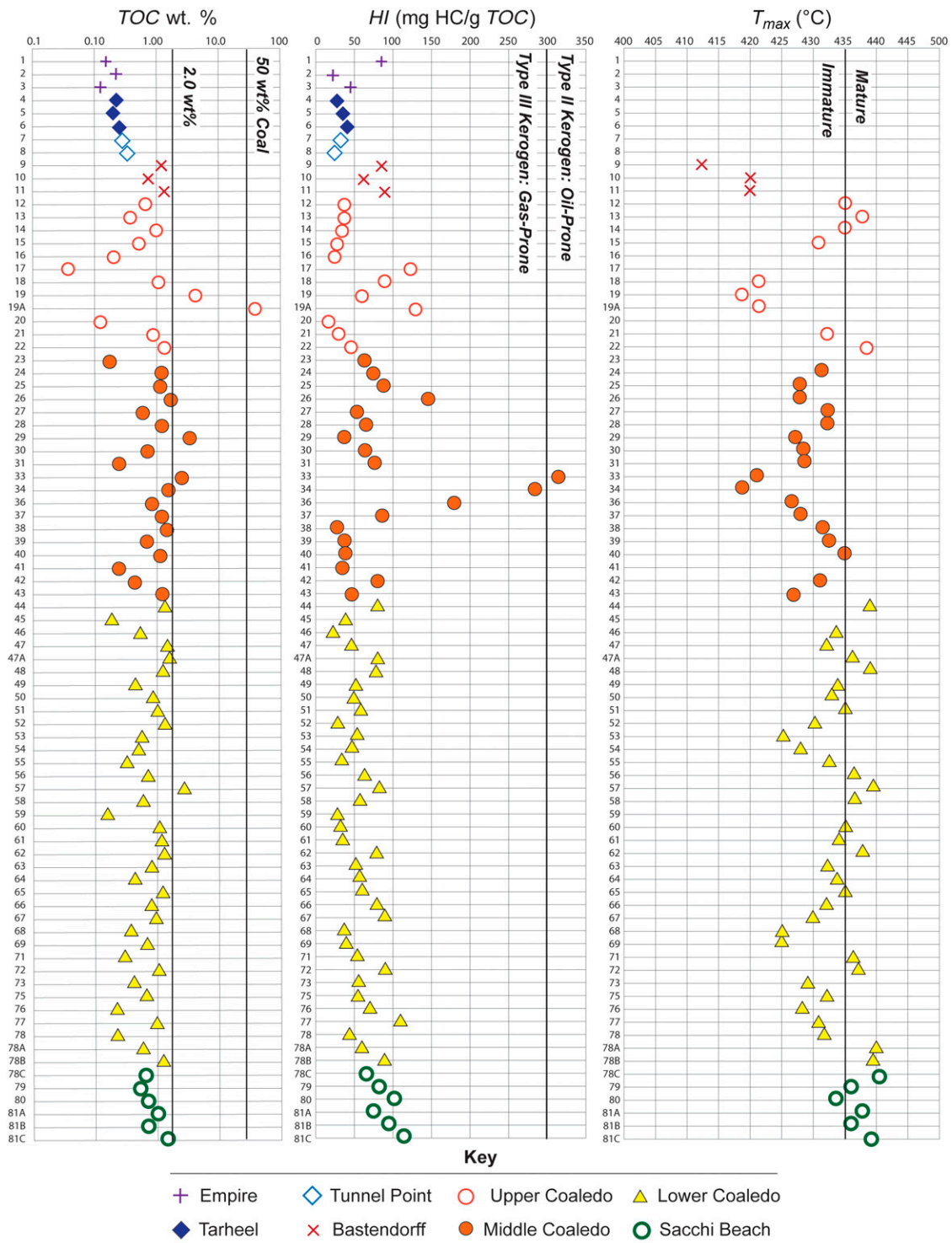


Figure 7. Outcrop HAWK pyrolysis results showing richness (total organic carbon [TOC]), quality (hydrogen index [HI]), and thermal maturity (T_{max}), with corresponding thresholds marked to evaluate source potential. These data show that the Lower, Middle and Upper Coaledo Formations have samples that are organically rich. The middle member has the best-quality organic matter of the strata sampled. The Sacchi Beach, Upper Coaledo and the Lower Coaledo display the highest degree of thermal exposure. Samples filtered for their S_2 are not graphed for their T_{max} .

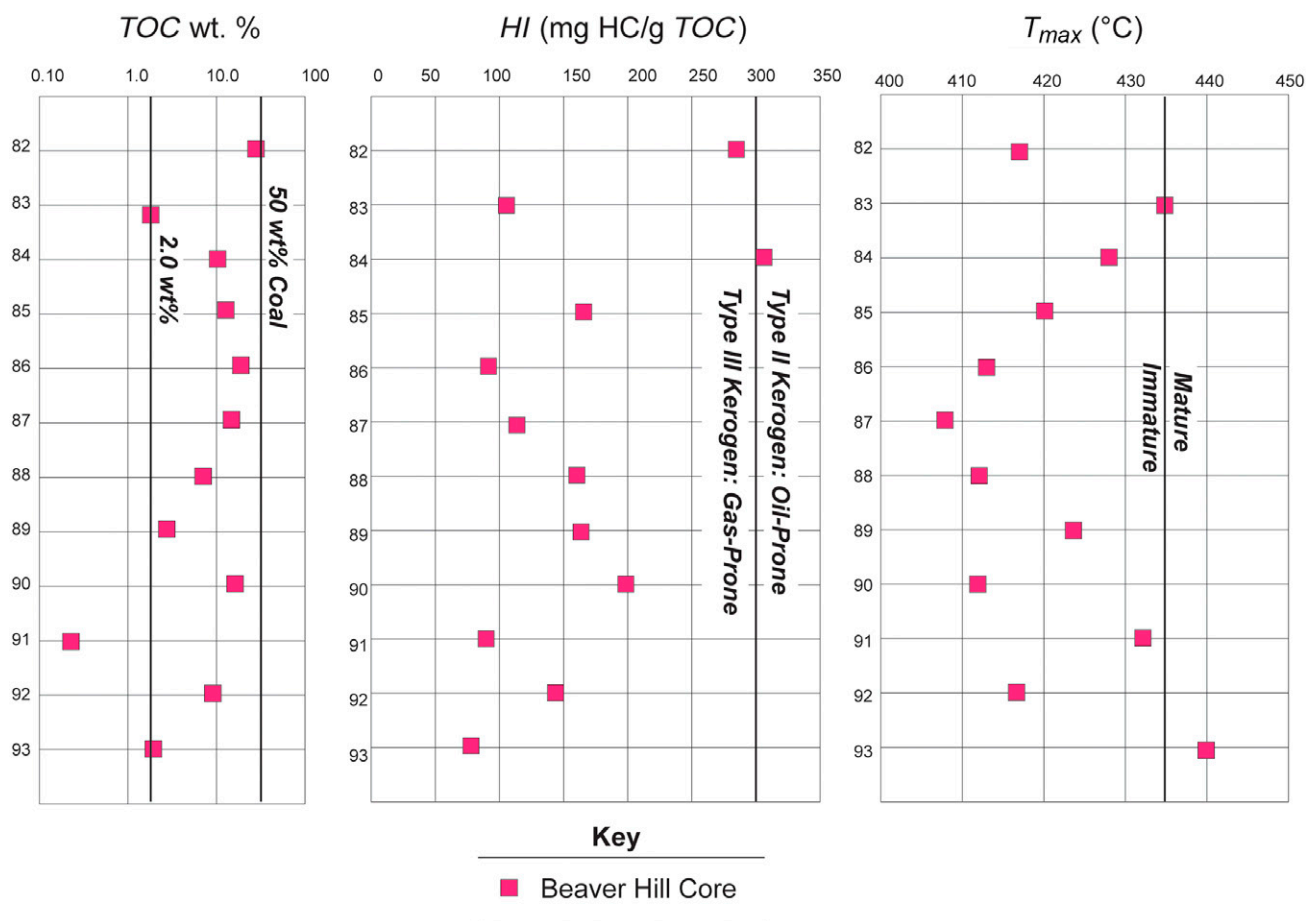


Figure 8. Beaver Hill core hole no. 1 HAWK pyrolysis results showing richness (total organic carbon [TOC]), quality (hydrogen index [HI]) and thermal maturity (T_{max}) with corresponding thresholds marked to evaluate source potential. The Lower Coaledo Formation core samples show that the organic matter is abundant, mostly gas prone, and mostly immature. Note the x axis scale change from the Figure 7 outcrop results.

and 33 in the Middle Coaledo, and sample 57 in the Lower Coaledo. Only one outcrop sample exceeds 50 wt. % (19A), and it is considered a coal.

All but one sample (91) in the Lower Coaledo core sample suite far exceeds the 2 wt. % threshold (Figure 8; Table 1); in fact the average TOC for the core samples is excellent, at 13% (Table 2). As previously mentioned, samples from the core were taken near coals from carbonaceous siltstones, which at times contained coal fragments (Figure 6).

Source Rock Quality

Source rock quality was established by characterizing the kerogen type of a sample, which was determined via the HI (Figures 7–9) and organic petrography (Table 1). Based on the original work of Espitalié et al. (1977) and further expanded on by Peters and

Cassa (1994), HI values <50 are kerogen type IV with no gas potential, values from 50 to 200 are kerogen type III and are gas prone, values of 200 to 300 are mixed oil and gas or type II–III kerogen, and values >300 are oil-prone type I–II kerogen.

The HI values from this study show that the majority of samples are type III kerogen or gas-prone source rocks, with the exception of samples 33 and 34, which are Middle Coaledo outcrop samples, and 82 and 84, which are Lower Coaledo samples from the BHC (Figure 9). Sample 84 was also classified as type II kerogen based on organic petrography. Organic petrography results similarly align with the HI results and show that the majority of samples are type III kerogen and are organic rich. These samples are rich in the terrigenous sourced detrohuminite maceral group, with minor, variable amounts of liptinite, a terrigenous and/or marine sourced maceral (Table 1).

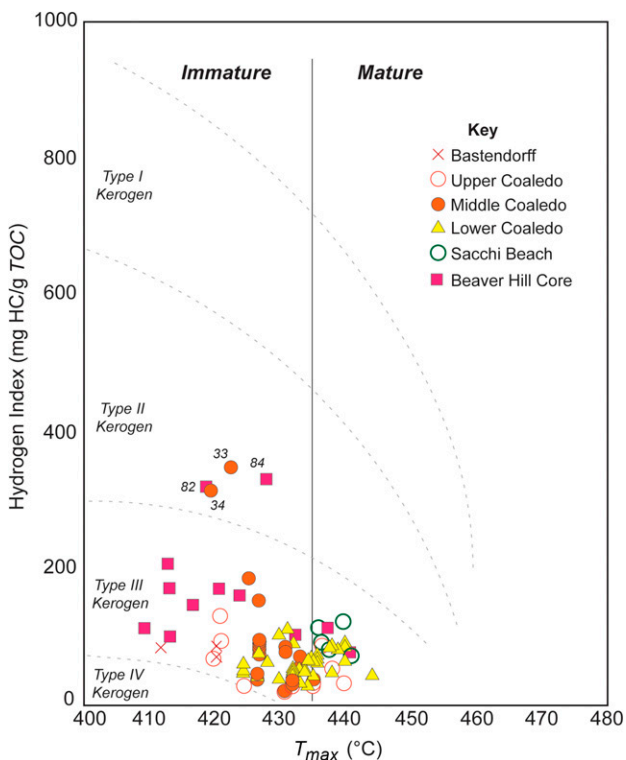


Figure 9. HAWK pyrolysis results mapped to show thermal maturity (T_{max}) versus hydrogen index to determine kerogen type. The Empire, Tarheel, and Tunnel Point samples had unreliable T_{max} , so their kerogen could not be determined via pyrolysis. Type III kerogen is likely to produce gas and types I and II kerogen liquid petroleum. Samples 33, 34, 82, and 84 are type II kerogen, whereas all of the other samples fall into the type III–IV kerogen category. Often, samples are a combination of kerogen types (I–IV); hence, when a sample nears a kerogen boundary, it is interpreted as a mix between its dominant kerogen type and whichever kerogen boundary the sample falls nearest. Most samples are generally immature, with the Sacchi Beach, Lower Coaledo, and portions of the Upper Coaledo marginally mature just above a T_{max} of 435°C.

Source Rock Potential

Richness and quality parameters clearly show that the Coaledo Formation has mudstone samples that exceed a TOC of 2 wt. %. Samples from the Lower Coaledo BHC contain siltstone that is very close to 50 wt. %, or a coal, and there are several coal seams indicated on the lithology log (Figure 6). The Middle Coaledo lacks coal but does have samples that near a TOC of 2.0 wt. % (samples 26 and 34) and samples that display TOC >2.0 wt. % (samples 29 and 33). The Upper Coaledo includes a 2-m coal seam that has a value of 52.3 wt. % (sample 19A). The quality of the organic matter in these rock samples has an

HI that is mostly <200, with a terrigenous organic makeup, so it is gas prone.

T_{max} of Source Rock

The T_{max} was determined from HAWK pyrolysis-derived T_{max} data, itself representing the peak temperature (°C) of the S_2 pyrolysis curve. Peters and Cassa (1994) suggest that a T_{max} of 435°C is the threshold for the onset of thermal maturity. The accuracy of the T_{max} measurement depends on the quality of the unimodal development of the S_2 peak and the amount of S_2 measured by the FID. Because of this, samples were filtered for their S_2 and their peak morphology; results are described in the following section.

Results indicate that the majority of Coos Bay rock units have T_{max} values measuring <435°C (Figures 7, 8), with the exception of 26 samples. These samples are in the Upper Coaledo (samples 12–14 and 22), Middle Coaledo (sample 40), Lower Coaledo (samples 46, 47A, 48, 51, 56, 57, 58, 60, 62, 65, 71, 72, 78A, and 78B), and two samples in the Lower Coaledo BHC (83 and 93). Conversely, in the Sacchi Beach, all of the samples measure >435°C, except sample 80, which measures just below the threshold, at 434°C. An additional column has been added to Table 1 showing equivalent petrographically measured % R_o results from Barbato et al.

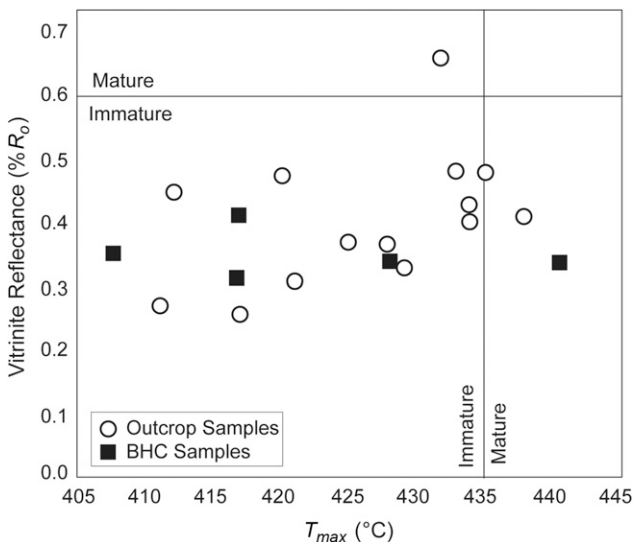


Figure 10. Crossplot of all of the samples with vitrinite reflectance (% R_o) data against thermal maturity (T_{max}) to show the range of T_{max} values compared to % R_o . The core samples range from 0.3% to 0.4% % R_o , with T_{max} values that range from 408°C to 440°C. BHC = Beaver Hill core hole no. 1.

Table 3. Comparisons between Outcrop and Core Free Hydrocarbon and Remaining Generative Potential Values

	Outcrop	Core	% Difference
Averages of all samples			
S_1	0.141	0.309	54.4
S_2	1.53	14.8	89.6
Averages of coal-associated samples			
S_1	0.327	0.502	35.0
S_2	23.6	27.4	14.1
Averages of shale, mudstone, and claystone samples			
S_1	0.064	0.203	68.5
S_2	0.826	18.4	95.5

The bulk of the disparity is attributed to differences between the shaly samples. Abbreviations: S_1 = free hydrocarbon; S_2 = remaining generative potential.

(data not shown). Crossplots of HI versus T_{max} and $\%R_o$ versus T_{max} (Figures 9, 10) also indicate that the majority of the samples are thermally immature. It is noted that a number of samples throughout the outcrop sample suite are only a few degrees shy of 435°C (Table 1, e.g., sample 80).

The T_{max} was further converted into a VRE value using the Jarvie 2001 equation. The VRE thermal maturity values reported in Table 1 are based upon the terminology outlined in Dembicki (2017), including immature-early oil (<0.6%), early oil (0.6%–0.8%), and late oil (1.0%). In summary, VRE results identify the same 26 samples identified by the T_{max} approach, which places them in the early oil-generation range. The VRE identifies 17 additional samples in the early oil-generation range in the Upper Coaledo (21), Middle Coaledo (27, 28, and 39), Lower Coaledo (46, 47, 49, 50, 55, 61, 63, 64, 66, 75, and 78), the Lower Coaledo BHC (91), and Sacchi Beach (80).

Pyrograms

This case-by case hierarchical filtering process yielded 81 viable T_{max} values from our 96 total samples. All 81 samples display pyrograms that exhibit sufficient unimodality and/or near-Gaussian distributions with limited skewness and kurtosis (i.e., Figure 11A). All Empire, Tarheel, and Tunnel Point outcrop T_{max} values were discarded because their pyrograms displayed visually bimodal peaks, peaks with appreciable skewness, negative kurtosis, and all $S_2 < 0.15$ mg HC/g rock. Three samples from the Upper Coaledo,

two samples from the Middle Coaledo, and two samples from the Lower Coaledo outcrops were discarded for the same reasons. All of the core samples displayed $S_2 > 0.15$ mg HC/g rock and S_2 peaks with sufficient unimodality. The S_2 peaks from the core samples were the most well-developed peaks seen in our entire sample suite.

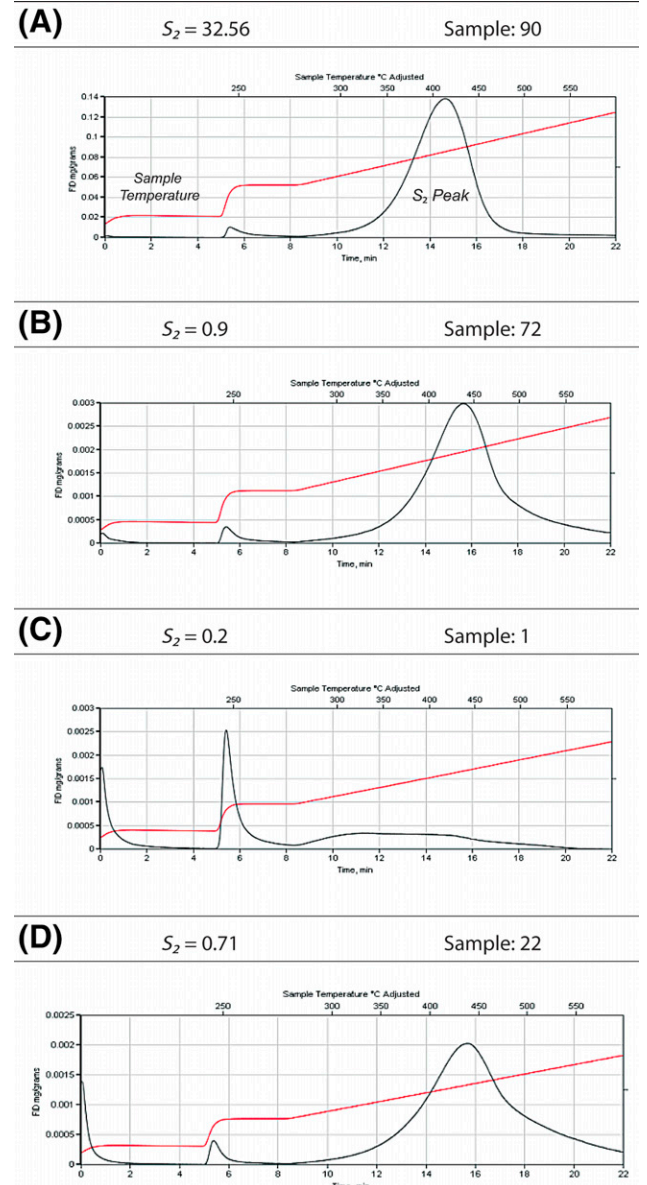


Figure 11. Examples of pyrograms generated from HAWK pyrolysis that display (A) a Gaussian distribution with $S_2 > 0.15$ mg HC/g rock, (B) a Gaussian distribution with $S_2 < 0.15$ mg HC/g rock, (C) a visually bimodally distributed peak displaying negative kurtosis and $S_2 = 0.20$ mg HC/g rock, and (D) a near-Gaussian distribution with S_2 approaching 1 mg HC/g rock, yet skewness is still easily observable. FID = flame ionization detector.

In general, lower values of S_2 correspond to poorly developed S_2 peaks; however, there are exceptions. Figure 11B shows an example in which $S_2 = 0.9$ mg HC/g rock, but the pyrogram clearly displays sufficient unimodality for the S_2 peak, so its T_{max} value is indeed accurate and should be used. In contrast, Figure 11C shows a sample in which $S_2 = 0.2$ mg HC/g rock, yet displays a clearly bimodal distribution exhibiting negative kurtosis, and its T_{max} value should be discarded. Lastly, results indicate that samples containing sufficient pyrolyzate, such as S_2 approaching 1 mg HC/g, fail to mean that their corresponding pyrograms will exhibit a perfect Gaussian distribution (Figure 11D). Although the S_2 is well developed and its T_{max} value should be used, it is noted that S_2 peak skewness can still occur in samples with relatively high S_2 yields.

DISCUSSION OF ROCK UNIT GEOCHEMISTRY AND STRATIGRAPHY

There are eight sedimentary rock units identified in the Coos Bay area representing varying paleocoastal depositional environments (Figure 4), and the observed source rock characteristics are largely a function of these environments. To fully determine the potential for the Coos Bay strata to be an effective petroleum system and to hypothesize which intervals may have produced previously encountered gas, geochemical results (TOC and HI) were evaluated in the context of lithologic observations. This allows us to ultimately tie geochemical observations back to the paleodepositional geologic framework of the area (Figure 14). Pyrogram filtering resulted in 81 samples out of the original 96, whose S_2 , T_{max} , and HI values are viable. The majority of samples with poor S_2 peak development occur in younger sandstone outcrops (Tunnel Point, Tarheel, and Empire Formations), and their poor S_2 is likely a reflection of the low organic nature of high-energy sandstones.

Sedimentological descriptions of the Coos Bay stratigraphic units are described based upon a combination of published data and the senior author's personal observations during field excursions. Rock unit boundaries follow the maps of Allen and Baldwin (1944) as modified by Madin et al. (1995) and Wiley et al. (2015), with slight modifications based on current field work (Figure 1). For a review of stratigraphic nomenclature and issues of rock unit thickness and

mapping gradational boundaries, see Baldwin and Beaulieu (1973) and Armentrout (2021). Rock unit ages are from Darin et al. (2022) (Figure 3). Paleogene formation thicknesses are from the west limb of the South Slough syncline. The thicknesses of the Neogene Tarheel and Empire Formations are from the east limb (Figure 5) (Armentrout, 2021).

After lithology and kerogen chemistry are discussed, the degree of relative thermal exposure needs to be established. The regional tectonic framework and burial history are complex (Figures 3–5), and so T_{max} and VRE were both used to measure the thermal maturity of a sample. However, as previously stated, there are inherent difficulties with the conversion of T_{max} to VRE . Although the VRE data are still informative, the authors chose to prioritize the implications of T_{max} results in the Discussion sections, and VRE data as secondary.

To be considered an effective petroleum system, key relationships in these data must be identified. Stratigraphy with promising source potential ($TOC > 2.0$ wt. %) must also display adequate thermal exposure ($T_{max} > 435^\circ\text{C}$), and any produced HCs need to accumulate in a reservoir, where they are stored via an effective seal.

Basal Unconformity

The base of the Coos Bay middle Eocene section is inferred to be unconformable with the mapped Tye Formation east of the studied coastal outcrops (Baldwin, 1961; Bird, 1967). Along the coastal section of the oldest Eocene strata, the beds of Sacchi Beach are juxtaposed against the intruded Paleocene sandstone of Fivemile Point (≥ 55 Ma) south of the Fulmar Fault (Wiley et al., 2015). The Fulmar Fault (fault A of Snavely et al. [1981]) deformation zone is interpreted as the southwest boundary of the Siletzia Terrane (Snavely, 1987; Wiley et al., 2015). For practical purposes, this unconformity can be considered the discontinuity of Siletzia terrane accretion inferred to be circa 51–49 Ma (Wells et al., 2014), with Sacchi Beach strata deposited beginning at least by circa 45 Ma (Figures 3, 5).

The Beds of Sacchi Beach or the Sacchi Beach Member of Tye Formation

At Cape Arago, the middle Eocene beds of Sacchi Beach (ca. 45.5–44.5 Ma) are ~ 425 m (~ 1394 ft)

thick and composed of predominantly micaceous siltstone and laminated mudstone, with intermittent turbiditic sandstone and channel complexes. This section was interpreted as distal prodelta with a stratigraphically shallower nearer-shore complex of nested delta front channelized facies. Within the Coos Bay study area, the beds of Sacchi Beach thicken to at least 550 m (1800 ft). It is important to note that the coastal outcrops of the beds of Sacchi Beach (Wiley et al., 2015) were previously called the Elkton Siltstone (Baldwin et al., 1973; Dott and Bird, 1979).

Geochemical results of the Sacchi Beach mudstones indicate fair to good organic richness, with a mean TOC of 0.96 wt. % and an *HI* of 88 mg HC/g TOC (Table 2), indicating type III kerogens; this suggests that the samples may be nearer to the delta front in a less distal environment. All but one sample measures above a T_{max} of 435°C, and thus the majority of samples are thermally mature (Figures 7, 9; Table 1). These were the most mature samples seen in the entire sample suite, supported by both T_{max} and *VRE* results. Results for the Sacchi Beach suggest lean source rock for the generation of gas from the prodelta facies.

Lower Coaledo

The beds of Sacchi Beach are gradationally overlain by the Coaledo Formation. The middle Eocene Lower Coaledo (ca. 44.5–42.3 Ma) is ~570 m (~1870 ft) thick and is composed of fine to coarse lithic feldspathic sandstone with siltstone, mudstone, coal, and minor conglomerate. Subbituminous and lignite coal beds are reported from the northwest end of Sacchi Beach, where approximately seven thin coal seams occur sporadically. Previous studies by Chan (1985), Ryberg (1978), and Chan and Dott (1986) identified up to 10 coarsening-upward cycles within the Lower Coaledo (Figure 5). Sedimentary structures common to the Lower Coaledo include planar bedding, hummocky cross-stratification, trough, ripple, swale, low angle, and planar-tabular cross-stratification; dewatering structures, burrows, and flaser bedding; and intraformational mudstone clasts, concretions, scours, prograding tidal bars with toset mud drapes, and reactivation truncation of tidal-bundle topsets. These features constitute a wave and tidally influenced prodelta basin-margin facies shallowing to distributary channels with laterally adjacent shoreface facies, all correlative with the

inboard swampy coastal plain of the Coos Bay coal field.

Although a few Lower Coaledo mudstones are above 1–2 wt. % TOC and initially suggest a good source rock, the average richness of the sample suite is 0.89 wt. % (Table 2). The TOC weight percent values are generally higher in the offshore facies that transgress over the upper shoreline sandstones and then, in most cases, decrease up-section as the facies become sandier, reflecting shallowing paleowater depths. The *HI* values from all of the samples indicate type III, gas-prone kerogen. Samples taken from cycles 4, 3, 2, and 1 (Figure 5) have *HI* values that are uniformly low (Table 1). This is probably due to the ubiquitous bioturbation, suggesting well-oxygenated waters associated with wave mixing indicated by the interbedded hummocky and swale cross-bedded sandstones.

The Lower Coaledo mudstones are also generally immature; however, 16 samples spread throughout the sample suite measure above 435°C and exhibit a somewhat cyclical pattern of maturity. This is likely a result of oxidation in sandier units of the coarsening upward parasequence cycles. All 16 samples were taken from intervals that contained hummocky bedded, fine-grained sandstone (Figure 5). However, it may also be recycling of older, more thermally altered organic matter, or it may represent inconsistent variations of thermal exposure due to erratic tectonic activity during the middle Eocene (Figure 3). Results for the Lower Coaledo outcrop samples suggest lean source rock potential for the generation of gas.

Lower Coaledo, BHC No. 1

Mean TOC values of the BHC samples are 13.01 wt. % and mean *HI* values are 158 mg HC/g TOC (Table 2), indicating significant source rock potential. The kerogens are type II–III, with all T_{max} <435°C, except for sample 93, and the deepest sample taken at 1360 m (4457 ft), which has a T_{max} of 440°C. Newton (1980, p. 14) considered maturation models requiring 1800 m (6000 ft) of burial, significantly deeper than our results, which indicate at least 1350 m (4450 ft). Parameters for the resource assessment of this study differ from Newton's assessments, which suggest a deeper burial threshold for maturation and increased optimism for marine source rocks

from this study, which exhibit good (>1.0 wt. %) TOC. The coal rank is generally subbituminous in the Coos Bay area, suggesting that previously encountered gas may have also migrated from more deeply buried source rock facies.

Core samples were evaluated for their source rock characteristics, but their results were also compared to Lower Coaledo outcrop samples in an attempt to evaluate the presence and magnitude of geochemical discrepancies that can occur between subsurface and outcrop samples (Table 3).

Differences between S_1 and S_2 values are significant, and, as expected, the unweathered core data have a stronger geochemical response compared to outcrop data (Table 3). This overall discrepancy is easily observable when comparing all of the core samples to all of the outcrop samples (Table 3, Averages of All Samples), where there is an ~55% difference between S_1 values and an ~90% difference between S_2 values. The differences among S_1 are predominantly attributed to oxidation and/or organic material weathering out of the outcrop over the course of geologic time. However, the magnitudes of the discrepancies among S_2 are striking and suggest that weathering alone may not fully explain the disparities; lithology and depositional environments may also play a role.

Core samples were taken from carbonaceous shale intervals and intervals with coaly stringers (Figure 6), and outcrop samples were taken from mostly mudstones with instances of coaly fragments or stringers (Figure 5). When coal-associated samples (Table 3, Averages of Coal-Associated Samples) and shale samples are compared (Table 3, Averages of Shale, Mudstone, and Claystone Samples), it becomes clear that the differences in the shale samples constitute the bulk of the overall geochemical discrepancies observed between outcrop and core S_1 and S_2 values. The differences in S_2 may also be depositionally influenced inasmuch as outcrop shale samples generally represent distal to lower and middle shoreface facies, whereas core shale samples were deposited in a fluvial marsh setting.

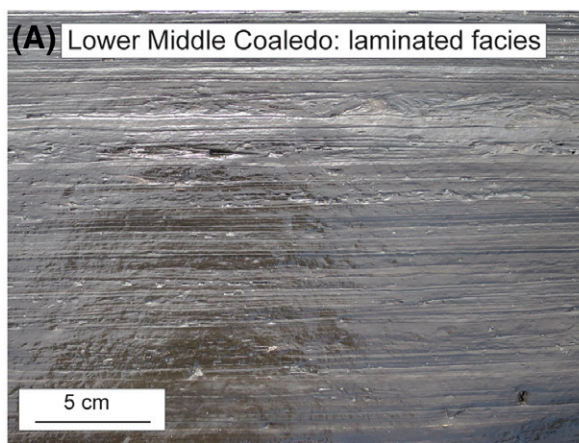
Despite the significant discrepancies, weathering and geologic processes did not “overprint” the outcrop samples to the point that good data could not be identified. The outcrop geochemistry data are still proportionally very good, as indicated by the well-developed S_2 peaks on the pyrograms that can be reliably used to identify potential source rock intervals.

Middle Coaledo

The late Eocene Middle Coaledo (ca. 42.3–41.2 Ma) is ~760 m (~2495 ft) thick and characterized by large intervals of laminated mudstone, massive mudstone, siltstone, and minor sandstone beds and two 10-m (30-ft)-thick intervals of fine-grained turbidite sandstones (Rooth, 1974). Stratigraphic lower and upper limits of the Middle Coaledo are gradational, with shoreface sandstone and mudstone intervals within the uppermost Lower Coaledo and lowermost Upper Coaledo (Figure 5). Observed sedimentary structures include plane laminated beds without bioturbations, suggesting poorly oxygenated intervals transitioning up-section to laminated intervals with numerous bioturbations associated with hummocky cross-stratification indicating normally oxygenated environments with significant wave energy. Stratal disruption includes rotated intervals tens of meters thick and “chaotic” intervals of gravity-flow events of primarily sand-beds sliding basinward (Armentrout, 2021). The Middle Coaledo extends southeastward as a transgressive interval, with muddy distal prodelta facies, between the predominantly sandy and coaly lower and upper Coaledo members.

The contrasting facies observed within the Middle Coaledo mudstones are, in part, reflected in the chemistry of the sample (Figure 12). The high TOC and HI values previously described occur within laminated facies that are essentially unbioturbated, suggesting possibly anoxic conditions with better preservation of the organic matter. In contrast, mudstones of sandy bioturbated facies higher in the section had a similarly high but slightly lower average TOC of 1.30 wt. %, and significantly lower average HI values of 82 mg HC/g TOC. This lower HI value suggests poorer preservation of organic matter in a higher-energy, sandy depositional environment, which likely led to the oxidation of organic material that would have constituted the S_2 .

Averaged Middle Coaledo mudstone samples have a TOC value of 1.24 wt. % and an HI mean of 94 mg HC/g TOC (Table 2), indicating overall organic-rich but low yield potential type III kerogen. However, samples 33 and 34 have markedly higher TOC values ranging from 1.83 to 2.26 wt. % and HI values ranging from 283 to 316 mg HC/g TOC, indicating at best a mixed type II–III prone kerogen (Figure 9). All of the samples are thermally



Sample	TOC	HI
33	2.26	316
34	1.83	283
36	0.9	173
37	1.23	86

Average TOC wt. % = 1.55

Average HI (mg HC/g TOC) = 214



Sample	TOC	HI
24	1.34	66
25	1.32	84
26	1.97	147
27	0.75	54
28	1.1	60

Average TOC wt. % = 1.30

Average HI (mg HC/g TOC) = 82

Figure 12. Lighthouse Beach facies contrasting (A) lower Middle Coaledo laminated facies and (B) upper Middle Coaledo sandy-bioturbated mudstone facies. Note the change in average hydrogen index (*HI*) from 214 to 82 in laminated versus bioturbated samples, and the slight decrease in total organic carbon (*TOC*) weight percent (wt. %).

immature, although it is noted that all of the samples are just a few degrees shy of the 435°C threshold (Table 1). Only one sample displays $T_{max} = 435^{\circ}\text{C}$ (Figure 7, sample 40).

Although results for the Middle Coaledo outcrop samples suggest minimal source rock potential, the laterally persistent mudstone facies of the members provide a top seal for Lower Coaledo sandstones.

Upper Coaledo

The late Eocene Upper Coaledo (ca. 41.2–39.5 Ma) is ~425 m (~1395 ft) thick and is composed of fine to coarse lithic feldspathic micaceous sandstone with pebbly sandstone siltstone, mudstone, coal, and minor conglomerate. The base of the Upper Coaledo is gradational, but it is most consistently marked at the base of thicker sandstones of the first prograding cycle

immediately west of the lowermost (western) sandstone point of Yoakam Point State Park. Chan and Dott (1986) identify up to eight coarsening upward cycles from prodelta-shelf facies shallowing to delta front facies. Within the Coos Bay coal field, as many as six to seven coal seams are recognized in the Upper Coaledo, including the Beaver Hill coal seam, which has been mined more than any other seam in the Coos Bay coal field and is correlated with the single coal that outcrops at Yoakam Point (Figure 13), with a local thickness of 1.5 to 2.7 m (Allen and Baldwin, 1944).

Table 2 shows moderately high average *TOC* values of 5.35 wt. %, and a mean *HI* value of 57 mg HC/g *TOC*, indicating limited source potential with type III kerogen, but there are also multiple samples displaying $HI < 50$, which are better classified as type IV kerogen. The *TOC* values are, as expected, very

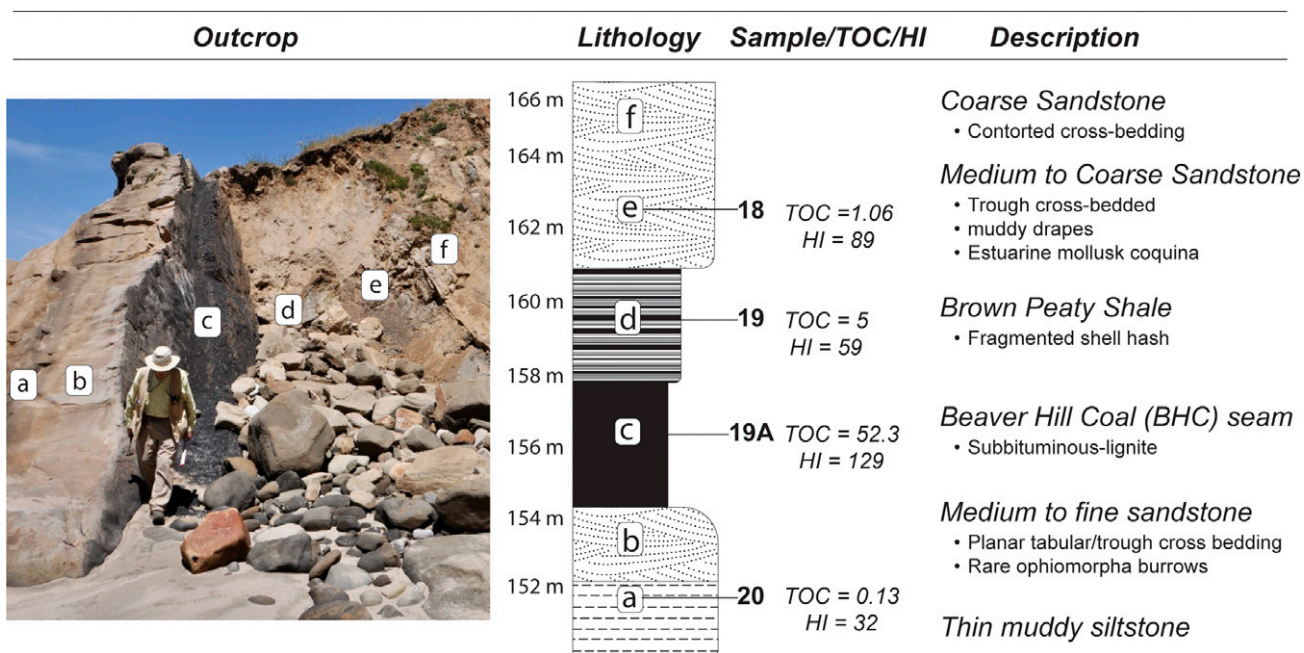


Figure 13. Outcrop photograph of the Beaver Hill coal seam, upper member, Coaledo Formation at Yoakam Point. Measured section of outcrop in meters (modified from Chan and Dott, 1986). Sample values for total organic carbon (TOC) and thermal maturity from Table 1. Depositional setting interpreted as upper shoreface to estuarine marsh. *HI* = hydrogen index.

low in the upper shoreface facies and elevated in estuarine marsh facies overlying the coal (Figure 13). Except for the coal, *HI* mean values are low, suggesting moderately well-oxygenated environments other than the densely compacting organics within the coaly marsh setting. Although the interval is organic rich, a little over half of the samples are thermally immature, and only 5 of the 12 samples are above the T_{max} threshold of 435°C, indicating a tendency toward moderate potential for the generation of gas, and the sandstone facies in the uppermost Upper Coaledo section indicate reservoir potential.

Bastendorff Shale

The uppermost Coaledo Formation sandstone is interpreted to be conformably overlain by the latest Eocene–early Oligocene Bastendorff Shale (ca. 39.5–33.5 Ma), which is ~950 m (~3120 ft) thick and dominantly finely laminated mudstone and thinly bedded siltstone with minor beds of fine-grained sandstone, tuffaceous siltstone, and water-laid tuff. Tipton (1975) provides the best description of the section; recovered foraminifera suggest deep basin-margin paleowater depths, with a midsection series of tabular fine-grained sandstones interpreted as

turbidites (Rooth, 1974; Armentrout, 2021). However, modern accretion of the Bastendorff Beach sands following emplacement of the Coos Bay South Jetty has resulted in a dense vegetational coverage over the mudstone section. Only three samples from a 9-m (30-ft) exposure represents the very thick, muddy Bastendorff facies.

Based on Tipton's (1975) deep-water interpretation, these mudstones would then be expected to have intervals of elevated richness and quality, similar to the Middle Coaledo laminated mudstone with elevated TOC and *HI* values, plus type II–III kerogens (Figures 9, 12). However, immature Bastendorff Shale samples have an average TOC value of 1.18 wt. %. The samples have an average *HI* value of 74 mg HC/g TOC (Table 2), indicating type III kerogens, and organic petrography also indicates type III kerogen. The *HI* and organic petrography therefore suggest that this section of the Bastendorff is a less distal environment, dissimilar from the Middle Coaledo. However, it is noted that limited access to outcrop exposures preclude truly representative sampling. Our ability to draw plausible conclusions regarding source rock potential or paleodepositional conditions from these data are, therefore, also limited. Still, the thick muddy Bastendorff Shale could

serve as a top seal rock for an Upper Coaledo sandstone reservoir.

Tunnel Point Sandstone

Gradationally above the upper Bastendorff silty mudstone lies the early Oligocene Tunnel Point Sandstone (ca. 33.5–30? Ma), which is ~245 m (~804 ft) thick and composed of tuffaceous fine-grained sandstone with sandy siltstone and thin wave-winnowed and often fossiliferous pebbly sandstone beds. The general lack of fine bedding suggests bioturbation. A molluscan fauna recovered from the Tunnel Point indicates a fully oxygenated marine environment of <60 m (<200 ft) paleowater depth, similar to the comparable fauna of the Eugene Formation (Hickman, 1969). The uppermost Tunnel Point is faulted and slumped and is overlain across the Coos Head fault by the Late Miocene Empire Formation with an apparent angular discontinuity of 12° (Weaver, 1945; Madin et al., 1995). The Early–Middle Miocene Tarheel Formation is unknown on the northeast limb of the South Slough syncline.

The Tunnel Point Sandstone has a mean TOC value of 0.45 wt. %; however, T_{max} and HI could not be accurately determined for these samples because their pyrograms were poorly developed and/or their S_2 values were insufficient. The organic petrography results provide insight and reveal type III kerogen material, which is expected for a well-oxygenated bioturbated sandy environment (Figures 7, 9). Results for the Tunnel Point Sandstone indicate minimal organic richness, and this section is better classified as a potential reservoir.

Oligocene–Miocene Unconformity

Beginning in the middle Oligocene, the Coos Bay Paleocene section (ca. 45–30 Ma) was deformed by regional southwest-northeast (modern coordinates) compression (Thompson et al., 2019; Darin et al., 2022). This deformation formed the northwest-southeast-trending South Slough syncline in which the Neogene strata were deposited (Figures 2, 3). Initiation of this deformation is interpreted at circa 33 Ma based on zircon populations (Darin et al., 2022). This compressive upper plate deformation, and possibly underplating, caused uplift of the southern Coast Range propagated northeastward, progressively separating the forearc into subregional Neogene

depocenters by right-lateral strike-slip faults and clockwise rotation driven by basin/range westward extension and northward compression by the San Andreas transform (Wells et al., 2017; Darin et al., 2022).

The importance of this unconformity is the uplift and erosion of the Paleogene section, resulting in less postunconformity–Neogene total burial depth and thermal exposure of the potential source rocks in the Sacchi Beach and Coaledo stratal units. Subsequent burial of the Paleogene section by the Neogene Tarheel and Empire units with a probable combined maximum thickness of 1350 m (4420 ft) likely would not have increased the T_{max} (°C) levels in the middle Eocene organic-rich mudstone.

Tarheel Formation

The Tarheel Formation (ca. 18?–15 Ma) is ~75 to a speculative 600 m (~246–1960 ft) thick, and is a fossiliferous, concretionary, lithic wacke exposed along the eastern shoreline of the Coos Bay shipping channel (Armentrout, 1967, 2021). Outcrops expose only 75 m of section, but projection of mapped formation boundaries from Madin et al. (1995) and dredged-fossil occurrences reported by Moore (1963) suggest possibly 600 m of section (Armentrout, 2021). This Miocene unit was recognized from a molluscan fauna dredged from the shipping channel in the 1940s (Moore, 1963), with outcrops discovered much later (Armentrout, 1967). The molluscan fauna suggests 50- to 100-m (160- to 330-ft) paleowater depth with fully marine conditions. Tarheel sandstones are highly bioturbated, but where bedding is observed, there are laminates of leaf fragments.

As with the Tunnel Point Sandstone, T_{max} and HI could not be accurately determined for these samples because their pyrograms were poorly developed and/or their S_2 values were insufficient. Silty sandstones of the Tarheel have a low mean TOC value of 0.29 wt. %, and organic petrography indicates type III kerogen. Results for the Tarheel Formation indicate minimal organic richness, and this section is also better classified as a potential reservoir.

Middle Miocene Unconformity

Tarheel sandstones are overlain by the Empire Formation (ca. 11.5?–7? Ma) with an angular discontinuity

(Armentrout, 1967, 2021). The angular discordance between the Tarheel Formation and the overlying Empire Formation is 13°–15° along the shipping channel north of Barview, with parallel northwest-southeast strikes suggesting continued Neogene folding along the same southwest-northeast (modern coordinates) upper plate compression (Thompson et al., 2019). The uppermost Tarheel and the overlying Empire Formation sandstone zircon samples are only 3–4 m (9–12 ft) stratigraphically apart and bracket a time gap of approximately 3 m.y., but probably less because this does not account for how much upper Tarheel was eroded (Armentrout, 2021; Darin et al., 2022).

Approximately 20° of Middle Miocene folding across the South Slough syncline resulted in an estimated uplift and erosion of 425 m (1400 ft) (L. Thompson, 2022, personal communication). The uplift and erosion associated with this unconformity negates sufficient burial of the Paleogene section to elevate thermal exposure of middle Eocene organic-rich strata, at least within the onshore area of the South Slough syncline.

Empire Formation

The Late Miocene Empire Formation (ca. 11.5–5? Ma) is ~750 m (~2460 ft) thick in the type section along the northeast limb of the South Slough syncline. On the southwest limb, the Empire is 450 m (1480 ft) thick and has been interpreted to unconformably overlie the Tunnel Point Formation, with an angular discordance of ~50°, but the relationship is complicated by the Coos Head Fault and local landslides (Allen and Baldwin, 1944; Weaver, 1945). The Empire is a massive, micaceous, bioturbated, fossiliferous, fine to medium-grained quartzo-feldspathic wacke, with minor siltstone, conglomerate, and a water-laid tuff dated at circa 8.2 Ma (Darin et al., 2022). The molluscan fauna suggests no more than 50–100 m (160–650 ft) paleowater depths (Armentrout, 1967).

Similar to the sandstone facies of the Tunnel Point and Tarheel units, T_{max} and HI could not be accurately determined for these samples because their pyrograms were poorly developed and/or their S_2 values were insufficient. Limited Empire Formation samples have low TOC mean values of 0.21 wt. %, and the kerogen is type III, as determined by

organic petrography. Results for the Empire Formation indicate minimal organic richness, and this section is better classified as a potential reservoir.

Post-Empire Unconformity

The Empire Formation dips 23° on both limbs of the South Slough syncline, indicating continued southwest-northeast compression after circa 5 Ma (Thompson et al., 2019; Darin et al., 2022). Strata unconformably overlying folded Empire sandstones include the Pliocene (?) Coos Conglomerate (D. Blackwell, 2023, personal communication) and marine terraces of Quaternary age (McInnelly and Kelsey, 1990). The estimate of Empire Formation erosion resulting from the late Neogene–Quaternary folding is 200 m (650 ft) (L. Thompson, 2022, personal communication), further limiting burial of middle Eocene strata to higher thermal exposure within the onshore South Slough syncline.

Quaternary Deformation

McInnelly and Kelsey (1990) and Kelsey et al. (1996) have studied the late Quaternary deformation of the Cape Arago-Bandon area identifying uplift and faulting of five marine platforms. These platforms are deformed by open folding and flexural-slip reverse faults. The youngest platform, Whisky Run, is well preserved along Cape Arago and has an estimated age of 80 ka. Deformation of this platform ranges from subsidence to a maximum uplift rate of 0.8 m/k.y. (McInnelly and Kelsey, 1990). This ongoing structural deformation along the Oregon-Washington coast raises the question of trap integrity of potential reservoir rock sands.

DISCUSSION OF GEOCHEMISTRY AND PALEOENVIRONMENTS

Paleogene deposition occurred within a stable shelf margin basin superimposed upon the accreted Siletzia terrane (Santra et al., 2013; Wells et al., 2014; Armentrout et al., 2021). HAWK pyrolysis data and results from organic petrography investigations indicate that the kerogen evaluated in Coos Bay Paleogene rock units ranges from terrigenous to marine (Figure 14; Table 1). Relevant geochemical and organic petrography results for each of the eight rock

units were integrated and placed based on geochemical parameters described in Peters and Cassa (1994) and its paleogeographic context (see the section Coaledo Delta Development and Paleogeography), which incorporates sedimentary descriptions and observations (Figure 14).

Paleogeographic reconstructions constrained by middle Eocene paleotransport directions suggest that the Coos Bay area of the postcollisional Paleocene basin deltaic-to-turbiditic deposition was directed generally slightly west of north (Dott, 1966; Dott and Bird, 1979; Chan and Dott, 1986; Blackwell et al., 2021). This paleogeographic reconstruction and sediment transport direction suggests that optimal burial history for mature offshore organic-rich sediments may be beneath the thick offshore down-dip extension of the South Slough syncline that projects northwest (modern coordinates).

In general, the geochemistry data align well with lithologic paleodepositional interpretations. However, the range of *HI* and S_2/S_3 for the BHC, cover a wide variety of environments, and both types II and III kerogen were identified via pyrolysis and organic petrography (Figure 9; Table 1). The results in Table 1 indicate ranges from lacustrine to distal marine. Curiously, sample 82, which has a *TOC* weight percent approaching that of a coal, displays an *HI* value that places it in the type II kerogen and distal marine category. These observations suggest that the BHC section of the Lower Coaledo may represent a more complex range of paleodepositional environments that merits further investigation into its kerogen.

The type II–III kerogen organic-rich rarely bioturbated and mostly laminated lower Middle Coaledo mudstone facies suggests possible anaerobic sea floor conditions. The predominantly riverine discharge of

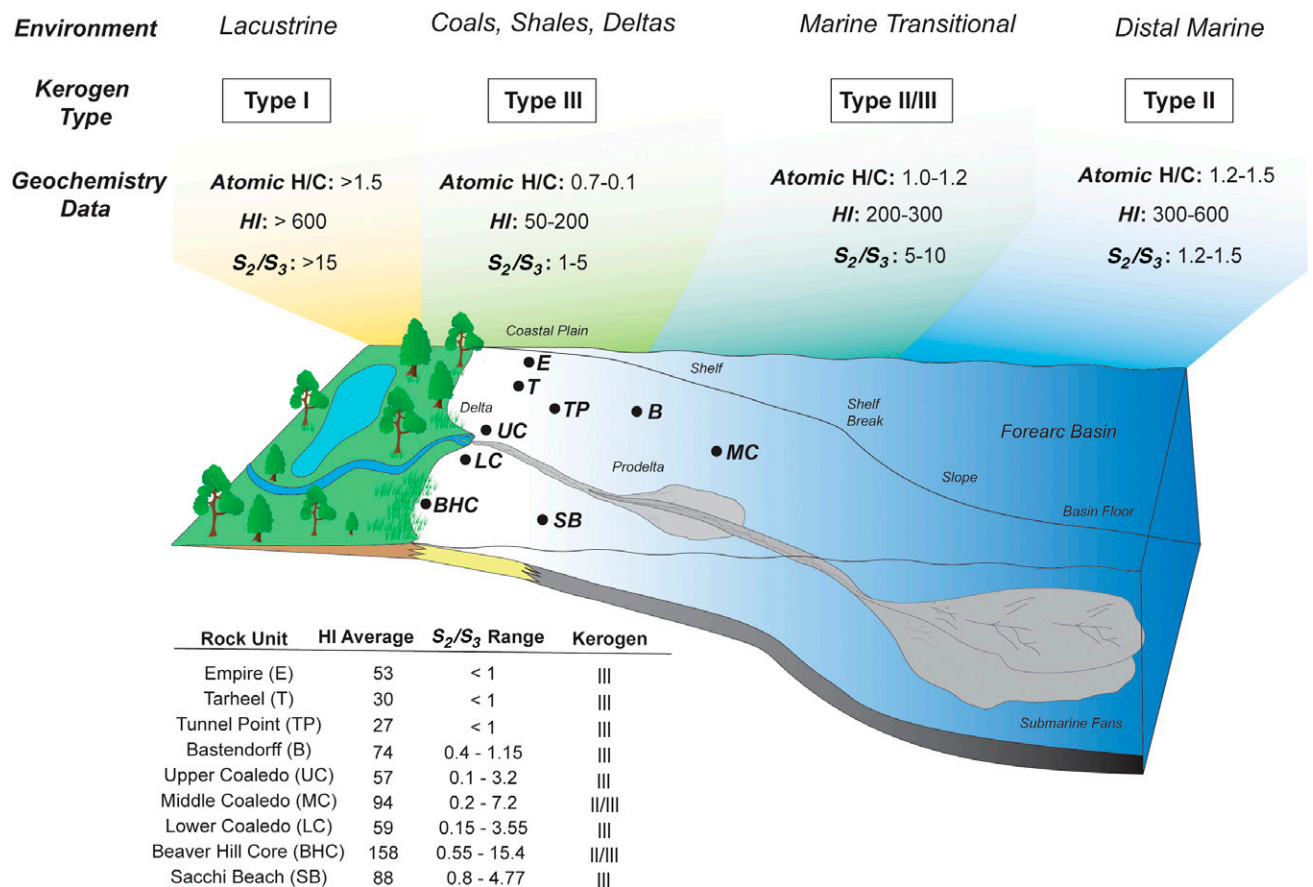


Figure 14. Generalized forearc basin depositional model, showing depositional environments with their corresponding kerogen types and HAWK pyrolysis ranges for hydrogen index (*HI*), remaining generative potential (S_2)/trapped CO_2 (S_3) and atomic H/C. Values are based on the ranges provided by Peters and Cassa (1994). The black circles on the model represent average *HI* and S_2/S_3 values for each of the eight Coos Bay Rock units and BHC. Samples with $S_2/S_3 = 0$ are interpreted to have lost a significant amount of S_1 due to weathering. This model builds on Figure 4, the paleogeographic figure constructed by Dott and Bird (1979).

organic matter into low oxygen settings seems a reasonable model for the laminated mudstones within the lower Middle Coaledo and perhaps the Bastendorff Shale. However, the Middle Coaledo results place it slightly further offshore compared to the Bastendorff, but again, Bastendorff sampling was sparse. Both units are relative transgressive systems that suggest reduced sediment influx to the shelf basin, reducing dilution of the organic matter (Gross, 1967; Seiter et al., 2004). Deeper zones of the postcollisional Paleogene basin may have periodically become anaerobic, with high preservation of organic-rich mudstone with HC yield potential.

SUMMARY AND CONCLUSIONS

Shelf-margin depositional systems are globally recognized for their potential to create effective petroleum systems. A total of 84 outcrop and 12 core samples evaluated from the wave-dominated middle-late Eocene Coaledo Delta, and its associated prearc to forearc shelf-margin depositional units, indicate intervals with lean to moderate gas-prone source rock potential. Geochemical parameters used to characterize source rocks are *TOC* weight percent (richness), T_{max} (maturity), and *HI* (quality), supported by organic petrography.

1. Rock Units with Source Potential: The Lower and Upper Coaledo contain coal seams and organic-rich siltstone that are the most prospective gas-prone source rock intervals (Figures 7–9; Tables 1, 2). The beds of Sacchi Beach also display potentially lean, gas-prone source rock potential. The Sacchi Beach and Lower Coaledo exhibit the highest degree of thermal exposure in the sample suite. However, the sample suite is generally immature, and thus previously encountered gas may have also migrated from depth.
2. *TOC* Weight Percent and *HI*: The highest *TOC* weight percent values are in laminated mudstones and lower *TOC* weight percent values are in well-oxygenated bioturbated mudstones, but *HI* appears to be more affected than *TOC* weight percent (Figure 12). Mudstone and coaly source rocks with good (1–2 wt. % *TOC*) to

excellent (>4 wt. % *TOC*) richness occur in distal shoreface to offshore mudstone and in marginal to nonmarine siltstones associated with coal (Figures 7–9, 12; Table 2). The *HI* indicates that the sample suite is dominated by type III kerogen.

3. Determining T_{max} : When evaluating the unimodality of S_2 peaks on pyrogram data to accurately determine the T_{max} of a sample, a blanket S_2 threshold may lead to incorporating poor data or tossing out good data (see the section Pyrograms; Figure 11). Hierarchically filtering S_2 peaks by statistical parameters such as bimodality, skewness, kurtosis, and unimodality in combination with an S_2 threshold of 0.15 mg HC/g rock proves to be an effective approach.
4. Outcrop versus Core Geochemistry: The magnitude of difference between S_1 and S_2 values between outcrop and core geochemistry is striking, with S_1 values showing an ~55% difference and S_2 values showing an ~90% difference (Table 3). The chemical difference between shales constitutes the bulk of the disparity, whereas the coal-associated samples display less variance. Discrepancies in S_1 are attributed to weathering and oxidation, but the magnitude of the S_2 discrepancy suggests additional influences, such as lithology and depositional environments. Despite these differences, the outcrop geochemistry data remain well preserved enough to reliably identify potential source rock intervals.
5. Additional Elements of the Petroleum System: Newton (1980, p. 14) considered maturation models requiring 1800 m (6000 ft) of burial, significantly deeper than our results, which indicate at least 1350 m (4450 ft). Parameters for the resource assessment of the present study differ from Newton's assessments, which suggest a deeper burial threshold for maturation and increased optimism for marine source rocks from this study that display good (>1.0 wt. %) *TOC*. The uppermost Upper Coaledo, Tunnel Point, Tarheel, and Empire are rock units displaying reservoir potential, whereas the Middle Coaledo and Bastendorff rock units may provide effective seals. Seal integrity is questionable due to historic and ongoing regional structural deformation (Figure 3).

Offshore exploration wells drilled along the Oregon coast in the 1960s identified gas at depth, but the lack of regional source potential and maturation trends discouraged further exploration interest in the region. The data presented in this study, along with the resulting paleogeographic model, suggest a reevaluation of the exploration model and source rock potential for Coos Bay, and merit a deeper look into the kerogen for the onshore to offshore Coos Bay area.

REFERENCES CITED

- Allen, J. E., and E. M. Baldwin, 1944, Geology and coal resources of the Coos Bay quadrangle, Oregon: Oregon Department of Geology and Mineral Industries Bulletin 27, 171 p., accessed August 1, 2022, <https://pubs.oregon.gov/dogami/B/B-027.pdf>.
- Akkutlu, I. Y., and Fathi, E., 2012, Multiscale gas transport in shales with local kerogen heterogeneities, *SPE Journal*, v. 17, no. 04, p. 1002–1011, doi:10.2118/146422-PA.
- Armentrout, J. M., 1967, The Tarheel and Empire Formations—Geology and paleontology of the type sections, Coos Bay, Oregon, Master's thesis, University of Oregon, Eugene, Oregon, 155 p.
- Armentrout, J. M., 2021, Tectonics and paleogeography of a post-accretionary forearc basin, Coos Bay area, SW Oregon, USA, in A. M. Booth and S. L. Grunder, eds., From terranes to terrains: Geological field guides on the construction and destruction of the Pacific Northwest: Boulder, Colorado, Geological Society of America Field Guide 62, p. 187–243, doi:10.1130/2021.0062(06).
- Armentrout, J. M., D. L. S. Blackwell, L. Thompson, M. Darin, K. McDougall, R. J. Weldon, and S. Bogue, 2021, Initiation and Cenozoic evolution of the Cascadia Forearc Basin: Multidisciplinary evidence from the Coos Bay area Cenozoic stratigraphy, southwestern Oregon: Geological Society of America Annual Meeting, Portland, Oregon, October 10–13, 2021, doi:10.1130/abs/2021AM-369448.
- Armentrout, J. M., and D. H. Suek, 1985, Hydrocarbon exploration in western Oregon and Washington: AAPG Bulletin, v. 69, no. 4, p. 627–643, doi:10.1306/AD46254C-16F7-11D7-8645000102C1865D.
- ASTM, 2015, D2797 standard practice for preparing coal samples for microscopical analysis by reflected light, petroleum products, lubricants, and fossil fuels; gaseous fuels; coal and coke, Sec. 5, V. 05.06, X p., accessed January 1, 2022, <https://www.astm.org/d7708-14.html>.
- Baldwin, E. M., 1961, Geologic map of the lower Umpqua River area, Oregon: Denver, Colorado, US Geological Survey Oil and Gas Investigation Map OM-204, scale 1:62,500, 1 sheet, doi:10.3133/om204.
- Baldwin, E. M., J. D. Beaulieu, L. Ramp, J. Gray, V. C. Newton, Jr., and R. S. Mason, 1973, Geology and mineral resources of Coos County, Oregon. Portland, Oregon, Oregon Department of Geology and Mineral Industries Bulletin 80, 93 p., accessed February 1, 2020, <https://pubs.oregon.gov/dogami/B/B-080.pdf>.
- Bindeman, I. N., J. S. Lackey, R. Jicha, and J. M. Armentrout, 2021, Searching for Yellowstone plume versus Cascade arc signatures in 49–30 Ma basaltic and rhyolitic rocks of western Oregon: Geological Society of America Annual Meeting, Portland, Oregon, October 10–13, 2021, doi:10.1130/abs/2021AM-368323.
- Bird, K. J., 1967, Biostratigraphy of the Tyee Formation (Eocene), southwestern Oregon, doctoral dissertation, University of Wisconsin, Madison, Wisconsin, 209 p.
- Blackwell, N., D. L. S. Blackwell, S. Bogue, R. Weldon, and J. M. Armentrout, 2021, Cenozoic evolution of the Cascadia forearc: Constraints from paleomagnetism and anisotropy of magnetic susceptibility of sedimentary rocks exposed near Cape Arago, central Oregon Coast: Geological Society of America Annual Meeting, Portland, Oregon, October 10–13, 2021, doi:10.1130/abs/2021AM-370501.
- Brownfield, M., 2011, Total petroleum systems and geologic assessment of undiscovered hydrocarbon resources in western Oregon and Washington province, in M. Brownfield, R. R. Charpentier, T. A. Cook, T. R. Klett, R. M. Pollastro, C. J. Schenk, P. A. Le, and GIS Spatial Data Team, eds., Geologic assessment of undiscovered hydrocarbon resources of western Oregon and Washington Province: Boulder, Colorado, US Geological Survey, 107 p., doi:10.3133/ds69X.
- Carvajal-Ortiz, H., and T. Gentzis, 2015, Critical considerations when assessing hydrocarbon plays using Rock-Eval pyrolysis and organic petrology data: Data quality revisited: *International Journal of Coal Geology*, v. 152, p. 113–122, doi:10.1016/j.coal.2015.06.001.
- Chan, M. A., 1985, Correlations of diagenesis with sedimentary facies in Eocene sandstones, western Oregon: *Journal of Sedimentary Petrology*, v. 55, no. 3, p. 322–333, doi:10.1306/212F86B6-2B24-11D7-8648000102C1865D.
- Chan, M. A., and R. H. Dott Jr., 1986, Depositional facies and progradational sequences in Eocene wave-dominated deltaic complexes, southwestern Oregon: *AAPG Bulletin*, v. 70, no. 4, p. 415–429, doi:10.1306/94885723-1704-11D7-8645000102C1865D.
- Curiale, J. A., and J. B. Curtis, 2016, Organic geochemical applications to the exploration for source-rock reservoirs—A review: *Journal of Unconventional Oil and Gas Resources*, v. 13, p. 1–31, doi:10.1016/j.juogr.2015.10.001.
- Curzon Energy, 2022, Coos Bay – Coal bed methane, accessed June 1, 2021, <http://www.curzonenergy.com/projects/asset-overview>.
- Darin, M. H., J. M. Armentrout, and R. J. Dorsey, 2022, Oligocene onset of uplift and inversion of the Cascadia forearc basin, southern Oregon Coast Range, USA: *Geology*, v. 50, no. 5, p. 603–609, doi:10.1130/G49925.1.
- Dembicki, J. H., Jr., 2017, Source rock evaluation, in J. H. Dembicki Jr., ed., *Practical petroleum geochemistry for exploration and production*: New York, Elsevier, p. 61–133, doi:10.1016/B978-0-12-803350-0.00003-9

- Diller, J. S., 1901, Coos Bay folio, Oregon: Geologic atlas of the United States: Boulder, Colorado, US Geological Survey, 13 p.
- Dorsey, R., M. Darin, J. Armentrout, M. Santra, D. L. S. Blackwell, and I. Bindeman, 2021, Tectono-stratigraphic evolution of SW Oregon from early Eocene collision of Siletzia to the modern Cascadia convergent margin: Geological Society of America Annual Meeting, Portland, Oregon, October 10–13, 2021, doi:10.1130/abs/2021AM-367232.
- Dott, R. H. Jr., 1966, Eocene deltaic sedimentation at Coos Bay, Oregon: *Journal of Geology*, v. 74, no. 4, p. 373–420, doi:10.1086/627175.
- Dott, R. H. Jr., and K. J. Bird, 1979, Sand transport through channels across an Eocene shelf and slope in southwestern Oregon, U.S.A., in L. J. Doyle and O. H. Pilkey, eds., *Geology of continental slopes*: Tulsa, Oklahoma, SEPM Special Publication 27, p. 327–342, doi:10.2110/pec.79.27.0327.
- Espitalié, J., 1986, Use of Tmax as a maturation index for different types of organic matter: Comparison with vitrinite reflectance, in J. Burrus, ed., *Thermal modeling in sedimentary basins*: Paris, Editions Technip, p. 475–496.
- Espitalié, J., M. Madec, B. Tissot, J. J. Mennig, and P. Leplat, 1977, Source rock characterization method for petroleum exploration, Offshore Technology Conference, Houston, Texas, May 1–4, 1977, doi:10.4043/2935-MS.
- Gao, Q., J. Liu, Y. Huang, W. Li, R. Shi, Y. K. Leong, and D. Elsworth, 2022, A critical review of coal permeability models: *Fuel*, v. 326, 125124, 17 p., doi:10.1016/j.fuel.2022.125124.
- Gross, M. G., 1967, Organic carbon in the surface sediment from the northeast Pacific Ocean: *International Journal of Oceanography and Limnology*, v. 1, no. 1, p. 46–54.
- Haykus, J., 1980, Appendix G. Results of organic maturation analysis, Geochem Job No. 1575, in V. C. Newton, ed., *Prospects for oil and gas in the Coos Basin, western Coos, Douglas, and Lane Counties, Oregon*, Oil and Gas Investigation Volume 6: Portland, Oregon, Oregon Department of Geology and Mineral Industries, p. 70–73.
- Heller, P. L., and P. T. Ryberg, 1983, Sedimentary record of subduction to forearc transition in the rotated Eocene basin of western Oregon: *Geology*, v. 11, no. 7, p. 380–383.
- Hickman, C. J. S., 1969, The Oligocene marine molluscan fauna of the Eugene Formation in Oregon: *University of Oregon Natural History Museum Bulletin*, no. 16, 112 p.
- International Committee for Coal and Organic Petrology, 2001, The new inertinite classification (ICCP System 1994): *Fuel*, v. 80, no. 4, p. 459–471, doi:10.1016/S0016-2361(00)00102-2.
- Jarvie, D. M., B. L. Claxton, F. Henk, and J. T. Breyer, 2001, Oil and shale gas from the Barnett Shale, Ft. Worth Basin, Texas (abs.): AAPG Annual Convention, Denver, Colorado, June 3–6, 2001, accessed September 1, 2019, <https://www.searchanddiscovery.com/abstracts/html/2001/annual/abstracts/0386.htm>.
- Katz, B. J., and F. Lin, 2021, Consideration of the limitations of thermal maturity with respect to vitrinite reflectance, Tmax, and other proxies: *AAPG Bulletin*, v. 105, no. 4, p. 695–720, doi:10.1306/09242019261.
- Kelsey, H. M., R. L. Tichnor, J. G. Bockheim, and C. E. Mitchell, 1996, Quaternary upper plate deformation in coastal Oregon: *GSA Bulletin*, v. 108, no. 7, p. 843–860, doi:10.1130/0016-7606(1996)108<0843:QUPDIC>2.3.CO;2.
- Law, B. E., D. E. Anders, T. D. Fouch, M. J. Pawlewicz, M. R. Lickus, and C. M. Molenaar, 1984, Petroleum source rock evaluations of outcrop samples from Oregon and northern California: *Oregon Geology*, v. 46, no. 7, p. 77–81.
- Lewan, M. D., 1987, Petrographic study of primary petroleum migration in the Woodford Shale and related rock units, in B. Doligez, ed., *Migration of hydrocarbons in sedimentary basins*: Collection colloques et séminaires: Paris, Editions Technip, p. 113–130.
- Madin, I. P., G. W. McNelly, and H. M. Kelsey, 1995, Geologic map of the Charleston Quadrangle, Coos County, Oregon: Portland, Oregon, Oregon Department of Geology and Mineral Industries Map GMS-94, scale: 1:24,000, 1 sheet, accessed August 20, 2021, <https://pubs.oregon.gov/dogami/gms/GMS-094.pdf>.
- Magoon, L. B., and W. G. Dow, eds., 1994, *The petroleum system—From source to trap*: AAPG Memoir 60, 655 p., doi:10.1306/M60585.
- McNelly, G. W., and Kelsey, H.M., 1990, Late Quaternary Tectonic deformation in the Cape Arago–Bandon region of coastal Oregon as deduced from wave-cut platforms. *Journal of Geophysical Research*, v. 95, no. B5, p. 6699–6713, doi:10.1029/JB095iB05p06699.
- Moore, E. J., 1963, Miocene mollusks from the Astoria Formation in Oregon: Washington, DC, US Geological Survey Professional Paper 419, 109 p.
- Newton, V. C., 1979, Oregon's first gas well completed: *Oregon Geology*, v. 41, p. 87–90.
- Newton, V. C., ed., 1980, *Prospects for oil and gas in the Coos Basin, western Coos, Douglas, and Lane Counties, Oregon*, Oil and Gas Investigation Volume 6: Portland, Oregon, Oregon Department of Geology and Mineral Industries, 17 p.
- Olmstead, D. L., 1985, Mist gas field: Exploration and development 1979–1984: Oil and Gas Investigation Volume 10: Portland, Oregon, Oregon Department of Geology and Mineral Industries, 40 p.
- Peters, K. E., 1986, Guidelines for evaluating petroleum source rock using programmed pyrolysis: *AAPG Bulletin*, v. 70, no. 3, p. 318–329, doi:10.1306/94885688-1704-11D7-8645000102C1865D.
- Peters, K. E., and M. R. Cassa, 1994, Applied source rock geochemistry: Chapter 5: Part II. Essential elements, in L. B. Magoon, and W. G. Dow, eds., *The petroleum system – From source to trap*: AAPG Memoir 60, p. 93–120.
- Pickel, W., J. Kus, D. Flores, S. Kalaitzidis, K. Christanis, B. J. Cardott, M. Misz-Kennan, et al., 2017, Classification of liptinite – ICOP system 1994: *International Journal of Coal Geology*, v. 169, p. 40–61, doi:10.1016/j.coal.2016.11.004.

- Profita, C., and T. Schick, 2022, Q&A: What are the chances of offshore oil and gas drilling in the Northwest?, accessed July 7, 2022, <https://www.opb.org/news/article/qa-what-are-the-chances-of-offshore-oil-and-gas-drilling-in-the-northwest/>.
- Ragan, B. A., McDougall, K., Armentrout, J. M., and Latendresse, P. A., 2023, Digital database of microfossil samples from southwestern coastal Oregon, accessed July 1, 2021, <https://www.sciencebase.gov/catalog/item/6453cc04d34eefd5da84382b>.
- Retallack, G. J., W. N. Orr, D. R. Prothero, R. A. Duncan, P. R. Kester, and C. P. Ambers, 2004, Eocene-Oligocene extinction and paleoclimatic change near Eugene, Oregon: GSA Bulletin, v. 116, no. 7, p. 817–839, doi:10.1130/B25281.1.
- Rooth, G. H., 1974, Biostratigraphy and paleoecology of the Coaledo and Bastendorff Formations, southwestern Oregon, doctoral dissertation, Oregon State University, Corvallis, Oregon, 270 p.
- Ryberg, P. T., 1978, Lithofacies and depositional environments of the Coaledo Formation, Coos County, Oregon, Master's thesis, University of Oregon, Eugene, Oregon, 159 p.
- Ryu, I.-C., 2008, Source rock characterization and petroleum systems of Eocene Tye Basin, southern Oregon Coast Range, USA: Organic Geochemistry, v. 39, no. 1, p. 75–90, doi:10.1016/j.orggeochem.2007.09.004.
- Santra, M., R. J. Steel, C. Olariu, and M. L. Sweet, 2013, Stages of sedimentary prism development on a convergent margin – Eocene Tye Forearc Basin, Coast Range, Oregon, USA: Global and Planetary Change, v. 103, p. 207–231, doi:10.1016/j.gloplacha.2012.11.006.
- Seiter, K., C. Hensen, J. Schröter, and M. Zabel, 2004, Organic carbon content in surface sediments – Defining regional provinces: Deep Sea Research Part I: Oceanographic Research Papers, v. 51, no. 12, p. 2001–2026, doi:10.1016/j.dsr.2004.06.014.
- Snavely, P. D. Jr., 1987, Tertiary geologic framework, neotectonics, and petroleum potential of the Oregon-Washington continental margin, in D. W. Scholl, A. Grantz, and J. G. Vedder, eds., Geology and resource potential of the continental margin of western North America and adjacent ocean basin – Beaufort Sea to Baja California, Earth Science Series v. 6: Santa Cruz, California, Circum-Pacific Council for Energy and Mineral Resources, p. 305–335.
- Snavely, P. D. Jr., H. C. Wagner, and N. S. MacLeod, 1964, Rhythmic-bedded eugeosynclinal deposits of the Tye Formation, Oregon Coast Range: Symposium on cyclic sedimentation: Kansas Geological Survey Bulletin, v. 169, p. 461–480.
- Snavely, P. D. Jr., H. C. Wagner, W. W. Rau, and D. Bukry, 1981, Correlation of Tertiary rocks penetrated in wells drilled on the southern Oregon continental margin: US Geological Survey Open-File Report 81-1351, 21 p., accessed March 1, 2021, <https://pubs.usgs.gov/of/1981/1351/report.pdf>.
- Stanley, R. G., 1991, Geologic basis for petroleum resource assessment of onshore western Oregon and Washington (Province 72): Reston, Virginia, US Geological Survey Open-File Report 88-450X, 31 p., accessed March 1, 2021, <https://pubs.usgs.gov/of/1988/0450x/report.pdf>.
- Stormberg, G. J., 1991, The Mist gas field, N.W. Oregon: Source rock characterization and stable isotope (C,H,N) geochemistry, M.S. thesis, Oregon State University, Corvallis, Oregon, 207 p.
- Sýkorová, I., W. Pickel, K. Christanis, M. Wolf, G. H. Taylor, and D. Flores, 2005, Classification of huminite – ICCP System 1994: International Journal of Coal Geology, v. 62, no. 1–2, p. 85–106, doi:10.1016/j.coal.2004.06.006.
- Taylor, G. H., M. Teichmüller, A. Davis, C. F. K. Diesse, R. Littke, and P. Robert, 1998, Coal petrology: Berlin, Gebrüder Borntraeger, 704 p.
- Thompson, L. B., J. M. Armentrout, and D. L. S. Blackwell, 2019, Tectonic history of the Coos Bay Basin and its relationship to Pacific Northwest 'Siletzia' tectonics: 2019 GSA Cordilleran Section, 115th Annual Meeting, Portland, Oregon, May 17–19, 2019, doi:10.1130/abs/2019CD-329361.
- Tipton, A., 1975, Foraminiferal biostratigraphy of the Late Eocene to Early Oligocene type Bastendorff Formation, near Coos Bay, Oregon, in D. E. Weaver, ed., Paleogene symposium and selected technical papers: Annual Meeting Pacific Sections AAPG, SEPM, Society of Exploration Geophysicists, Long Beach, California, April 21–24, 1975, p. 563–585.
- Turner, F. E., 1938, Stratigraphy and mollusca of the Eocene of western Oregon: Boulder, Colorado, Geological Society of America Special Paper 10, 130 p., doi:10.1130/SPE10-p1.
- Tybor, P., 1980, Appendix F. Results of organic maturation analysis, Geochem Job No. 1227, in V. C. Newton, ed., Prospects for oil and gas in the Coos Basin, western Coos, Douglas, and Lane Counties, Oregon. Oil and Gas Investigation Volume 6: Portland, Oregon, Oregon Department of Geology and Mineral Industries, p. 62–69.
- Van Atta, R. O., 1980, Appendix D. Petrography of thin sections from Pan American well OCS P-112, in V. C. Newton, ed., Prospects for oil and gas in the Coos Basin, western Coos, Douglas, and Lane Counties, Oregon, Oil and Gas Investigation Volume 6: Portland, Oregon, Oregon Department of Geology and Mineral Industries, p. 60–61.
- Weaver, C. E., 1945, Stratigraphy and paleontology of the Tertiary formations at Coos Bay, Oregon: Seattle, Washington, University of Washington Publications in Geology, v. 6, no. 2, p. 31–62.
- Wells, R. E., R. J. Blakely, A. G. Wech, P. A. McCrory, and A. Michael, 2017, Cascadia subduction tremor muted by crustal faults: Geology, v. 45, no. 6, p. 515–518, doi:10.1130/G38835.1.
- Wells, R. E., D. Bukry, R. Friedman, D. Pyle, R. Duncan, P. Haeussler, and J. Wooden, 2014, Geologic history of Siletzia, a large igneous province in the Oregon and Washington Coast Range: Correlation to the geomagnetic polarity time scale and implications for a long-lived Yellowstone hotspot: Geosphere, v. 10, no. 4, p. 692–719, doi:10.1130/GES01018.1.
- Wells, R. E., A. S. Jayko, A. R. Niemi, G. Black, T. Wiley, E. Baldwin, K. M. Molenaar, K. L. Wheeler, C. B. DuRoss,

- and R. W. Givler, 2000, Geologic map and database of the Roseburg 30' × 60' quadrangle, Douglas and Coos counties, Oregon: Menlo Park, California, US Geological Survey Open-File Report 00-376, 55 p., accessed December 1, 2021, https://pubs.usgs.gov/of/2000/0376/pdf/rb_geol.pdf.
- Wells, R. E., and A. R. Niem, 2021, Evolution of the Cascadia forearc of Oregon and Washington: Geological Society of America Annual Meeting, Portland, Oregon, October 10–13, 2021, doi:10.1130/abs/2021AM-366818.
- Wiley, T. J., J. D. McClaughry, C. A. Niewendorp, L. Ma, H. H. Herinckx, and K. A. Mickelson, 2015, Geologic map of the southern Oregon coast between Bandon, Coquille, and Sunset Bay, Coos County, Oregon: Portland, Oregon, Oregon Department of Geology and Mineral Industries Open File Report 0-15-04, 57 p., accessed January 1, 2022, <https://pubs.oregon.gov/dogami/ofr/p-O-15-04.htm>.
- Ziarani, A. S., and R. Aguilera, 2011, Knudsen's permeability correction for tight porous media: *Transport in Porous Media*, v. 91, no. 1, p. 239–260, doi:10.1007/s11242-011-9842-6.